

Description of the CLIO model version 3.0

by

Hugues Goosse, Jean-Michel Campin, Eric Deleersnijder, Thierry Fichet, Pierre-Phillipe Mathieu, Miguel Angel Morales Maqueda and Benoît Tartinville

*αγναν επισκοπε χερνιβων,
πολυλλιστον α τ αρυον-
τεσσι, χρυσοπεπλε Κλειοι,
παρεχειζ ενωδεζ αμβροσιων
εκ μυχων εραννον νδωρ,...*

*Overseer of the holy lustration-water, golden-
robed Clio, who give the water-drawers from
the ambrosial cave the fragrant lovely water
sought with many prayers, ...*

Simonides, c.a. 556 b.c.- 464 b.c.
Edited and translated by David A. Campbell

Contents

1. Introduction	4
2. The oceanic component	4
2.1. The governing equations	4
2.2. Parameterization of vertical mixing	7
2.3. Parameterization of downsloping currents	11
2.4. Barotropic and baroclinic modes	12
2.5. Time and space discretisation	14
3. The sea ice component	20
3.1. Vertical growth and decay	20
3.2. Lateral growth and decay of the ice	23
3.3. Ice dynamics	25
3.4. Horizontal transport	26
4. Coupling the oceanic and sea-ice components	27
4.1. Exchange of momentum	27
4.2. Exchange of heat	28
4.3. Exchange of mass	29
5. Boundary conditions and surface forcing	30
5.1. Surface flux of heat	30
5.2. Surface flux of freshwater	35
5.3. Surface flux of momentum and boundary condition for turbulent kinetic energy	37
5.4. Lateral and bottom boundary condition	38
6. The evolution of CFC	38
References	41

1. Introduction

The CLIO (Coupled Large-scale Ice Ocean) model has been developed to study the role of ice and ocean in the climate system. It results from the coupling of a sea-ice model and an ocean model both built at the Institut d'Astronomie et de Géophysique G. Lemaître, Louvain-la-Neuve (ASTR). The ocean model follows the work of Jean-Michel Campin and Eric Deleersnijder (Deleersnijder et al., 1993; Deleersnijder and Campin, 1995; Campin, 1997; Campin and Goosse, 1999) and the sea-ice model is the one developed by Miguel Angel Morales Maqueda and Thierry Fichefet (Morales Maqueda, 1995; Fichefet and Morales Maqueda, 1997, 1999)¹. The goal of the present note is to provide a summary of the major features of the model with a particular focus on the new points compared to previous versions.

2. The oceanic component

2.1. The governing equations

The equations governing large-scale geophysical flows are deduced from the Navier-Stokes equations written in a rotating frame of reference with some classical approximations (Gill, 1982; Cushman-Roisin, 1994; Campin, 1997) :

- the Boussineq approximation which states that the variation of the density ρ are small compared to its mean ρ_0 . It allows to replace the density by its reference value ρ_0 , except in the expression of gravitational force;
- the depth of the ocean is assumed negligible compared to the Earth's radius and the vertical depth scale is supposed much shorter than the horizontal one;
- the hydrostatic approximation, which leads directly to Eq. (3).

Those equations, written for the horizontal velocity \mathbf{u} ², the vertical velocity w , the potential temperature³ θ , and the salinity S , are :

the continuity equation :

$$\frac{\partial w}{\partial z} + \nabla_h \cdot \mathbf{u} = 0 , \quad (1)$$

the horizontal momentum equation :

$$\frac{\partial \mathbf{u}}{\partial t} + \mathbf{u} \cdot \nabla_h \mathbf{u} + w \frac{\partial \mathbf{u}}{\partial z} + f \mathbf{e}_z \times \mathbf{u} = - \frac{1}{\rho_0} \nabla_h p + \mathbf{F}_{du} , \quad (2)$$

the vertical momentum equation :

¹ It has been necessary to modify the horizontal grid of the sea-ice model to make it identical to the one of the ocean model. This transformation leads to only minor differences (Goosse, 1995).

² Vectors are represented by bold characters.

³ The potential temperature θ is defined as the temperature a water parcel would acquire if it was moved adiabatically to a reference pressure, usually the atmospheric pressure (Gill, 1982; Cushman-Roisin, 1994). The potential temperature is not modified in case of an adiabatic pressure change and is thus better adapted than in situ temperature to study the ocean over a wide range of depths.

$$\frac{\partial p}{\partial z} = -\rho g , \quad (3)$$

the equations for the evolution of θ and S :

$$\frac{\partial \theta}{\partial t} + \mathbf{u} \cdot \nabla_h \theta + w \frac{\partial \theta}{\partial z} = F_{d\theta} + F_{v\theta} , \quad (4)$$

$$\frac{\partial S}{\partial t} + \mathbf{u} \cdot \nabla_h S + w \frac{\partial S}{\partial z} = F_{dS} , \quad (5)$$

the equation of state:

$$\rho = \rho(\theta, S, z) . \quad (6)$$

t is the time, z is the vertical coordinate along axis \mathbf{e}_z , a unit vector directed upward, p is the local pressure and g is the gravitational acceleration ($g=9.8 \text{ m}^2/\text{s}$). The Coriolis parameter f is defined as:

$$f = 2\Omega \sin \varphi , \quad (7)$$

where Ω is the Earth's rotation frequency ($7.29 \times 10^{-5} \text{ s}^{-1}$) and φ is the latitude.

$F_{v\theta}$ is the volume source of temperature due to the absorption of solar radiation in the ocean interior (see sub-section 5.1.). In Eqs. (1) to (5), the notation $\nabla_h \cdot$ has been introduced for horizontal divergence and $\nabla_h(\)$ for horizontal gradients.

F_{du} , $F_{d\theta}$, and F_{dS} account for the effects of small-scale processes, not explicitly represented by the model. Regarding the momentum, a simple Laplacian formulation is retained (Bryan, 1969; Maier-Reimer et al. 1993; Drijfout et al., 1996):

$$\mathbf{F}_{du} = A_u \nabla_h^2 \mathbf{u} + \frac{\partial}{\partial z} \left(K_u \frac{\partial \mathbf{u}}{\partial z} \right) \quad (8)$$

where ∇_h^2 is the two-dimensional Laplacian operator. A distinction between vertical (K_u) and horizontal (A_u) viscosity is introduced to take into account the large difference of length scales between these two directions and the role of the strong vertical gradients of density in the reduction of vertical mixing in the ocean interior. The horizontal viscosity A_u are taken constant ($A_u=100\,000 \text{ m}^2/\text{s}$ in the coarse resolution and $20\,000 \text{ m}^2/\text{s}$ in the high resolution version). The value of A_u is chosen to ensure the numerical stability of the model and is much too high for representing realistically the physical processes. The way K_u and \mathbf{u} is computed is developed in the sub-section 2.2.

For the parameterization of the effect sub-grid scale processes on scalar quantities s (S or θ), the model relies on both the isopycnal mixing formulation (Redi, 1982), using the approximation of the small slopes (Cox, 1987), and the eddy-induced advection term ($\mathbf{u}^*, \mathbf{w}^*$), as proposed by Gent and Mc Williams (1990) (see also sub-section 2.2). Both parameterizations intend to represent the effects of quasi-horizontal meso-scale eddies that are too small (typical size from 10 to 100 km) to be explicitly resolved by the model:

$$F_{ds} = A_s \nabla_h^2 s + \nabla \cdot (\mathbf{K}_I \cdot \nabla s) + \frac{\partial}{\partial z} \left(K_s \frac{\partial s}{\partial z} \right) - u^* \nabla_h s - w^* \frac{\partial s}{\partial z} \quad (9)$$

\mathbf{K}_I refers to the isopycnal mixing tensor:

$$\mathbf{K}_I = A_i \begin{pmatrix} 1 & 0 & \alpha^x \\ 0 & 1 & \alpha^y \\ \alpha^x & \alpha^y & (\alpha^x)^2 + (\alpha^y)^2 \end{pmatrix} \quad (10)$$

with α^x , α^y the isoneutral slope in the x and y direction :

$$\alpha^x = \frac{\partial \rho}{\partial x} / \left(\frac{\partial \rho}{\partial z} \right)_p \quad (11)$$

$$\alpha^y = \frac{\partial \rho}{\partial y} / \left(\frac{\partial \rho}{\partial z} \right)_p$$

The bolus velocity (u^*, w^*) is simply derived from the stream function :

$$(u^*, v^*) = \nabla \times \psi \quad (12)$$

with

$$\begin{cases} \psi_x = -A_{gm} \alpha^y \\ \psi_y = A_{gm} \alpha^x \\ \psi_z = 0 \end{cases} \quad (13)$$

where A_{gm} is the thickness diffusion. This formulation ensures that (u^*, w^*) satisfy the continuity equation. In the coarse resolution version, standard values for A_i and A_{gm} are 300 m²/s and 200 m²/s, respectively. In the high resolution version, standard values for A_i and A_{gm} are 150 m²/s and 100 m²/s, respectively. A small horizontal diffusivity ($A_h = 50$ m²/s in the coarse resolution version, $A_h = 25$ m²/s in the high resolution version) is maintained for stability reason (Beckers et al, 1998).

It is imposed that the slope is always lower than $\alpha_{max} (= 10^{-2})$ in order to prevent cross directional diffusion fluxes from exceeding the stability criteria (Mathieu, 1998). Furthermore, to account for the transition toward surface mixed layer process, a gradual reduction of the eddy induced transport is achieved in the surface layers, according to Large et al (1997) approach. The stream-function ψ (or the diffusion thickness A_{gm}) is reduced by a factor gamma (gamma ≤ 1) :

$$gamma = 0.5 \{1 + \sin[\pi(r - 0.5)]\} \quad (14)$$

where r is the ratio of local depth, d and of the product of the slope α and the Rossby radius of deformation R :

$$r = \frac{d}{R|\alpha|} \quad (15)$$

The Rossby radius is evaluated from the Coriolis parameter f , according to $R = 2 / f$. In addition, it is imposed that R is comprised between 15 and 100 km.

The equation of state (6) follows Eckart (1958). This equation is a little less precise than that of the UNESCO (e.g., Gill, 1982) but is much less complex and needs a significantly smaller CPU time (Campin, 1997). It reads

$$\frac{1000.0}{\rho(T, S, z)} = 0.698 + \frac{1779.5 + (11.25 - 0.0745 T) T - (3.8 + 0.01 T) S}{p + 5890 + (38.0 - 0.375 T) T + 3.0 S} \quad (16)$$

where p (in atm) is computed by $p = 1 + \rho_0 g(-z)/101315$ with $\rho_0 = 1030$. The units are ρ (kg/m³), S (psu), T (°C), z (m).

Originally, Eckart's equation was given as a function of the in situ temperature T . Campin (1997) has introduced a simple correction to express it as a function of potential temperature :

$$T = \theta - \xi z \quad (17)$$

with $\xi = 9 \times 10^{-5}$ °C/m. This linearization of the relation between T and θ is similar to that performed by Maier-Reimer et al. (1993) for the UNESCO equation.

2.2. Parameterization of vertical mixing

The parameterization of vertical mixing used in CLIO (Goosse et al., 1999) follows the Kantha and Clayson's (1994) version of Mellor and Yamada's level 2.5 model (Mellor and Yamada, 1982).

The vertical viscosity and diffusivity are considered to be proportional to characteristic velocity (q) and length (l) of the turbulent motions:

$$K_u = l q S_u , \quad (18)$$

$$K_s = l q S_s . \quad (19)$$

S_u and S_s are stability functions (see below).

The turbulent velocity scale is defined as (Mellor and Yamada, 1974)

$$q^2 = \overline{u'^2} + \overline{v'^2} + \overline{w'^2} , \quad (20)$$

where u' , v' , w' are high frequency velocity fluctuations in the three directions and the overbar denotes an averaging over a suitable time scale. q^2 is thus twice the turbulent kinetic energy. When closure hypotheses are applied, the budget equation for q^2 reads (e.g., Mellor and Yamada, 1974, 1982) :

$$\frac{Dq^2}{Dt} = 2K_u M^2 - 2K_s N^2 - \frac{2q^3}{B_1 l} + \frac{\partial}{\partial z} \left(K_q \frac{\partial q^2}{\partial z} \right) \quad (21)$$

with

$$N^2 = -\frac{g}{\rho_0} \frac{\partial \rho}{\partial z}, \quad (22)$$

and

$$M^2 = \left| \frac{\partial u}{\partial z} \right|^2, \quad (23)$$

B_l is a constant whose value is given below (Eq. 28). The terms in the right-hand-side member represent respectively the transfer of energy from the mean current to the turbulence, the source or sink of turbulent energy associated with the exchanges with potential energy, the dissipation of turbulent energy, and the vertical diffusion. In this equation, advection and horizontal diffusion are not taken into account. Rosati and Miyakoda (1988), Deleersnijder (1992) or Blanke and Delecluse (1993) have demonstrated that those terms have a negligible role in the turbulent kinetic energy budget.

K_q is the vertical turbulent diffusion parameterized by :

$$K_q = l q S_q, \quad (24)$$

with $S_q = 0.2$ (Mellor and Yamada, 1982; Kantha and Clayson, 1994).

Following the arguments of Galperin et al. (1988), the stability functions S_u and S_s are only a function of

$$G_H = -\frac{l^2}{q^2} N^2, \quad (25)$$

which renders the model less prone to oscillations than its original version, in which the stability functions also depend on the current shearing (e.g., Deleersnijder and Luyten, 1994).

Kantha and Clayson (1994) propose the expressions:

$$S_s = \frac{A_2 \left(1 - 6 \frac{A_1}{B_1} \right)}{1 - 3A_2 G_H [6A_1 + B_2(1 - C_3)]}, \quad (26)$$

$$S_u = A_1 \left\{ \frac{\left[\left(1 - 6 \frac{A_1}{B_1} - 3C_1 \right) + 9[2A_1 + A_2 + (1 - C_2)] S_s G_H \right]}{(1 - 9A_1 A_2 G_H)} \right\}, \quad (27)$$

where the various constants, determined for the most part from laboratory experiments, are (Mellor and Yamada, 1982; Kantha and Clayson, 1994) :

$$(A_1, A_2, B_1, B_2, C_1, C_2, C_3) = (0.92, 0.74, 16.6, 10.1, 0.08, 0.7, 0.2). \quad (28)$$

Two realisibility conditions have to be imposed to avoid non physical results (Galperin et al., 1988; Kantha and Clayson, 1994) :

$$G_H \leq \left\{ A_2 [B_1 + 12A_1 + 3B_2(1 - C_3)] \right\}^{-1}, \quad (29)$$

$$\frac{N l}{q} \leq C_4, \quad (30)$$

where C_4 is 0.53, which gives a lower bound on G_H of -0.28. The above expression can also provide a limit for l :

$$l \leq C_4 \frac{q}{N}. \quad (31)$$

It is now necessary to specify the turbulence macroscale scale l , which is the characteristic size of the large turbulent eddies, i.e. those that contain most of the turbulent energy. One solution is to establish a new evolution equation for this length scale or any combination of q and l (e.g., Mellor and Yamada, 1974, 1982; Rodi, 1987). However, this approach implies that an additional differential equation must be solved. An alternative way is to prescribe l as an algebraic function (Gaspar et al., 1990; Blanke and Delecluse, 1993). Here, we use (Mellor and Yamada, 1982)

$$l = l_0 \frac{k L_d}{k L_d + l_0}, \quad (32)$$

where

$$L_d = \frac{d_s d_b}{d_s + d_b}. \quad (33)$$

d_s and d_b are the distances to the surface and the bottom, respectively, and k is the von Karman constant (=0.4). Close to the interface, l tends asymptotically to the well-known expression ("law of the wall") :

$$l = k L_d, \quad (34)$$

and l tends to l_0 away from the boundary. A lot of formulations have been proposed for l_0 (e.g., Mellor and Yamada, 1982), but for simplicity we have taken it as a constant ($l_0=10$ m)

We must stress that the value of l given by Eq. (27) is generally much larger than the limit imposed by Eq. (26). As a consequence, Eq. (27) only applies in slightly stratified regions or in unstable ones. Actually, our formulation of the mixing length is

close to that proposed by Blanke and Delecluse (1993) where l is proportional to q/N for stable density profile and to the local depth for unstable ones.

The scheme of Mellor and Yamada has been generally applied in models using a relatively high vertical resolution (e.g., Mellor et al., 1986; Oey and Mellor, 1993). No modification has been applied here to take into account the resolution being relatively coarse but it would be worth addressing this issue in the future.

The model described above applies only to fully turbulent regions like the surface mixed layer. In regions below, a minimum (background) diffusivity is imposed, following a vertical profile similar to that used by Bryan and Lewis (1979) (Fig. 1). The background viscosity is constant and equal to K_{ur} except above -150 m, where it increases upward, reaching 10^{-3} m²/s at surface (Campin, 1997).

The grid resolution and the approximations used to simplify the equations (mainly the hydrostatic approximation) do not allow to have an explicit description of the strong convection, that occurs, for example, in the Greenland Sea in winter (Killworth, 1983; Morawitz et al., 1996). Furthermore, Mellor-Yamada's model was not designed to work properly in these circumstances. This problem is generally tackled in OGCM by introducing a convective adjustment scheme. Some studies have demonstrated that one of the major consequences of the convection is an intense vertical mixing (Send and Marshall, 1995). As a consequence, the convective adjustment scheme applied here, similar to what has been used by Marotzke (1991) or Hirst and Cai (1994), consists in increasing of the vertical diffusivity whenever the profile is unstable. The value chosen for the diffusivity is 10 m²/s, which is within the range proposed by Klinger et al. (1996). As already stated by Hirst and Cai (1994), the model is not sensitive to this value (providing that it is not too small). In the present version, this convective adjustment is applied only if the instability reaches a depth greater than 100m because for shallower convection the turbulence scheme is assumed to do a reasonable job.

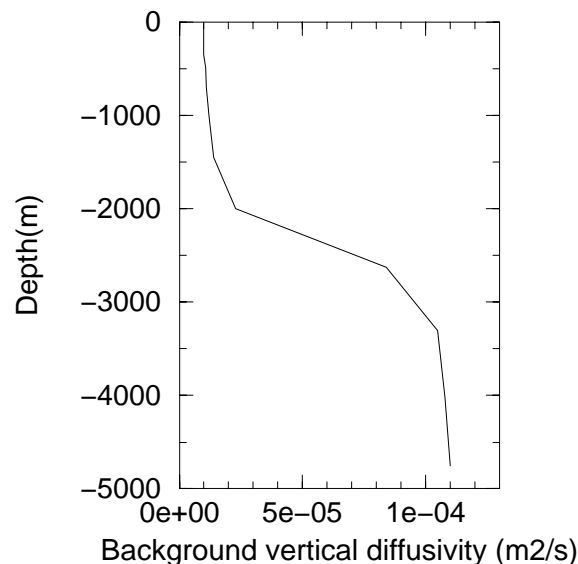


Fig.1 Vertical profile of background diffusivity. Units are m²/s.

2.3. Parameterization of downsloping currents

The dense water that flows out of the continental shelves and descends toward the bottom along the continental slope is thought to be a major source of deep water renewal (Killworth, 1983). For example, this mechanism seems to be very important for Antarctic Bottom Water (AABW) formation (Gill, 1973; Foster and Carmack, 1976; Gordon, 1991). The water gets denser on the Antarctic shelf because of strong ice production and thus brine release there (Gill, 1973). At the shelf break, this high salinity shelf water mixes with ambient pycnocline and deep waters and then sinks along the slope to form new bottom water (Foster and Carmack, 1976). However, these boundary plumes cannot be represented explicitly in coarse-resolution models⁴ because they have too small an extent (their characteristic thickness is of the order of 100 m; see for example the observations of Foldvik et al., 1985; Foster et al., 1987; Muench and Gordon, 1995). Furthermore, they can be strongly influenced by processes not simulated in large-scale models such as mesoscale eddy formation (Gawarkiewicz and Chapman, 1995; Jiang and Garwood, 1995, 1996) or by small-scale bathymetric features like canyons (Chapman and Gawarkiewicz, 1995; Jiang and Garwood, 1995).

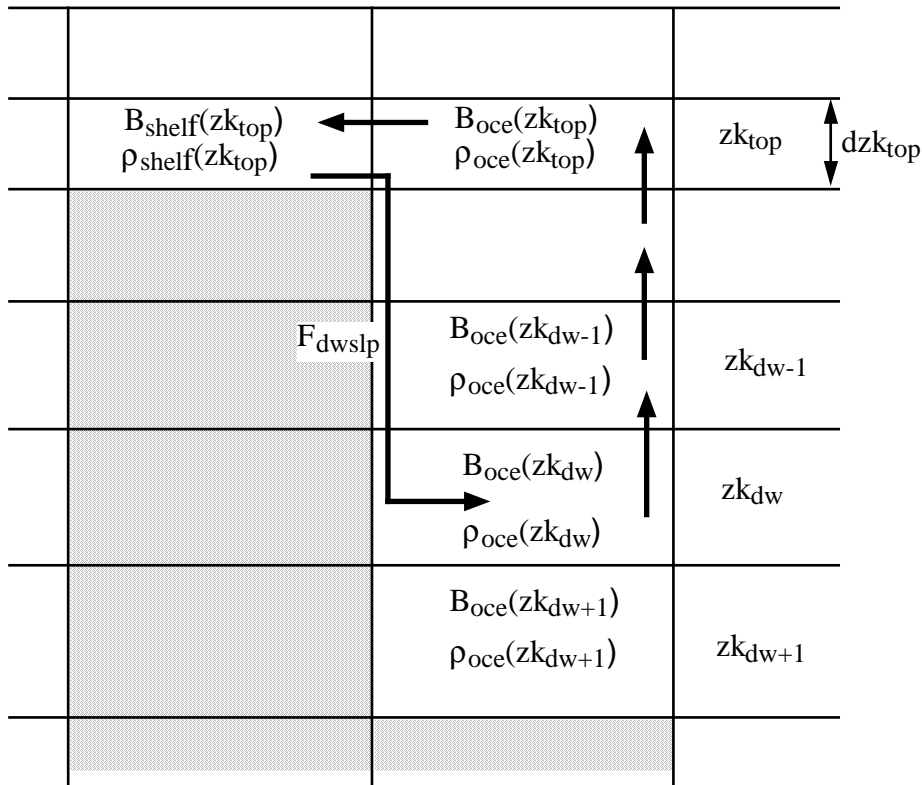


Fig.2 Schematic representation of the downsloping flow from the grid box $B_{shelf}(z_{k_{top}})$ to the grid box $B_{oce}(z_{k_{dw}})$ if the density on the shelf $\rho_{shelf}(z_{k_{top}})$ is higher than the density of the neighbouring ocean $\rho_{oce}(z_{k_{top}})$.

As a consequence, the effect of downsloping flow has to be parameterized. Several methods have been proposed recently (Harvey, 1996; Beckman and Döscher, 1997; Campin and Goosse, 1999). Here, the approach of Campin and Goosse (1999) has been adopted because it provides a simple and coherent way of dealing with downsloping currents in coarse-resolution models. The flow itself is not represented;

⁴Particularly in z-coordinate models where the slope is generally considered as a vertical wall.

only its impact on water properties is simulated. If the density $\rho_{shelf}(zk_{top})$ of a grid box $B_{shelf}(zk_{top})$ on the continental shelf⁵ (Fig. 2) is higher than the density $\rho_{oce}(zk_{top})$ of the neighbouring box $B_{oce}(zk_{top})$ over the deep ocean at the same depth, it induces a transport from the shelf towards the deep ocean with an intensity given by :

$$F_{dwsfp} = \gamma \Delta\rho dzk_{top} dy , \quad (35)$$

where γ is a coefficient ($\gamma=1.0$), $\Delta\rho=\rho_{shelf}(zk_{top})-\rho_{oce}(zk_{top})$ is the difference of density between the shelf and the ocean, and dzk_{top} and dy are the mesh sizes on the vertical and in the direction along the shelf break, respectively. $\gamma\Delta\rho$ can be interpreted as the velocity of the downsloping flow averaged over the size of the grid box, the velocity being proportional to $\Delta\rho$, the "driving force" of the current (Campin and Goosse, 1999).

The water is assumed to flow along the slope until it reaches a depth of equal density. The corresponding level k_{dw} is defined such that the local density⁶ of the water which comes from the shelf ρ'_{shelf} is higher than the density of the water at this level $\rho_{oce}(zk_{dw})$ but smaller than the density of the level below $\rho_{oce}(zk_{dw+1})$:

$$\rho'_{shelf}(zk_{dw}) \geq \rho_{oce}(zk_{dw}) \quad (36)$$

$$\rho'_{shelf}(zk_{dw+1}) < \rho_{oce}(zk_{dw+1}) \quad (37)$$

If the shelf water is denser than any water in the deep ocean, the shelf water is incorporated in the bottom level.

This transport from $B_{shelf}(zk_{top})$ to $B_{oce}(zk_{dw})$ must be compensated by a return flow in order to verify volume conservation. This is achieved by a transport, equal to F_{dwsfp} (Eq. 32), from $B_{oce}(zk_{dw})$ to $B_{oce}(zk_{dw-1})$ until $B_{oce}(zk_{top})$ and then to $B_{shelf}(zk_{top})$. Even though the real path is certainly much more complicated, this pattern seems more logical than a simple transfer from $B_{oce}(zk_{dw})$ to $B_{shelf}(zk_{top})$ since this kind of upwelling is unlikely to occur in the real ocean.

2.4. Barotropic and baroclinic modes

The fast external inertia-gravity waves with a speed of the order of 200 m/s (Gill, 1982; Cushman-Roisin, 1994) strongly constrain the time step allowed in the numerical resolution of the Eqs. (1) to (7). For a typical horizontal grid spacing of 10^5 m, the explicit resolution of these waves imposes a time step smaller than 10 minutes (e.g., Beckers and Deleersnijder, 1993), which is too small if long integrations (order of 1000 years) are necessary. Furthermore, it is not really useful to take into account those waves in climate studies. One classical solution to this problem (Bryan, 1969) is to eliminate these surface waves by considering that the surface is flat ("rigid lid" approximation).

⁵ The parameterization is described for a flow from the continental shelf toward the ocean, but this method is applied near any step in bathymetry.

⁶ This density is evaluated from the salinity and potential temperature of the shelf water at the corresponding depth.

An alternative formulation is used here, in which it is possible to keep the ocean surface free (Killworth et al., 1991; Deleersnijder and Campin, 1995; Campin, 1997). In order to have a CPU-time consumption similar to models using the "rigid lid" approximation (Killworth et al., 1991), the split-explicit method is applied (Gadd, 1978). The numerical resolution is decomposed into two parts: the depth-integrated part (hereafter termed barotropic mode) and the depth-dependent one with a zero vertical mean (baroclinic one). The low numerical-cost 2-D barotropic mode, which includes the surface gravity waves is integrated with a small time step (dtb), while the more expensive 3-D baroclinic mode is solved using a much longer time step ($dtu = M dtb$).

After a vertical integration of Eqs. (1) and (3), the equations for the barotropic mode read (Killworth et al., 1991; Deleersnijder and Campin, 1995; Campin, 1997):

$$\frac{\partial \eta}{\partial t} = -\nabla_h \cdot \mathbf{U} , \quad (38)$$

$$\frac{\partial \mathbf{U}}{\partial t} + f \mathbf{e}_z \times \mathbf{U} = -gH \nabla_h \eta + \mathbf{F}_U + A_u \nabla_h^2 \mathbf{U} . \quad (39)$$

η is the sea-surface elevation, H is the total depth and \mathbf{U} is the total transport :

$$\mathbf{U} = \int_{-H}^0 \mathbf{u} dz ,$$

where the reference level (called "0") is such that the average of η over the whole globe is zero. \mathbf{F}_U is a forcing term which involves only slow baroclinic terms or those with a smaller amplitude as the momentum advection:

$$\mathbf{F}_U = -\int_{-H}^0 \left(\frac{g}{\rho_0} \nabla_h \int_z^0 \rho d\zeta \right) dz + \int_{-H}^0 \left(-(\mathbf{u} \cdot \nabla_h) \mathbf{u} + A_u \nabla_h^2 \mathbf{u} - \frac{A_u}{H} \nabla_h^2 \mathbf{U} + \frac{\partial}{\partial z} K_u \frac{\partial \mathbf{u}}{\partial z} \right) dz . \quad (37)$$

M_2 time steps of the barotropic mode are performed (keeping \mathbf{F}_U constant) and then the baroclinic part is integrated by solving Eqs. (1) and (2). At a final stage, it is imposed that the depth-averaged velocity obtained by this latter step is equal to that obtained at the end of the barotropic computation. This method is simpler than solving directly an equation for a velocity having a zero vertical mean and then adding the barotropic part (Campin, 1997).

The number of integrations of the barotropic mode M_2 is not equal to M ($=dtu/dtb$) because η and \mathbf{U} are averaged over the last N_{av} iterations of the barotropic mode to smooth the fields (Campin, 1997). In order to keep a time consistency between the baroclinic and barotropic modes, N_{av} is chosen as $N_{av} = 2(M_2 - M) + 1$.

The values used in the coarse resolution version are :

$$\begin{aligned} dtb &= 5 \text{ minutes,} \\ dtu &= 3 \text{ hours,} \\ M &= 36, \\ M_2 &= 46, \\ N_{av} &= 21 . \end{aligned}$$

The values used in the high resolution version are :

$$dtb = 150 \text{ seconds,}$$

$$dtu = 90 \text{ minutes,}$$

$$M = 36,$$

$$M_2 = 46,$$

$$N_{av} = 21 .$$

2.5. Time and space discretisations

For the horizontal diffusion and advection terms involved in Eqs. (1) to (5), the time discretisation is based on a forward scheme⁷ while for the Coriolis term a semi-implicit method is used. Along the vertical, the small grid spacing, associated with the relatively strong diffusion coefficients, make it necessary to solve the time evolution of the various variables implicitly, in order to keep a reasonable time step. The time steps used for the resolution of barotropic and baroclinic modes have already been given above. In the equations for scalars (as well as for the turbulent kinetic energy), the time step dts is equal to 24 hours, which allows a good representation of the evolution of the ocean and is long enough to limit the CPU-time consumption of the model (keeping it stable). It should be necessary to perform 8 (dts/dtu) baroclinic time steps for one scalar time step in order to ensure the time consistency. However, the acceleration technique proposed by Bryan and Lewis (1979) and Bryan (1984) is applied. It consists in multiplying the left hand member of Eq. (3) by a coefficient $\delta = dts/dtu$ and then considering the same time step (dts) throughout the model. Killworth et al. (1984) have shown that this modification does not seem to cause problems in large-scale ocean models when the factor δ is smaller than 25. This method modifies the wave propagation (Bryan and Lewis, 1979; Bryan 1984), but it provides the advantage of reducing the total CPU-time consumption of the model by a factor 3. On the other hand, the time step for scalars is taken homogenous along the vertical because the technique used by Bryan and Lewis (1979) to accelerate the convergence of the deep ocean by increasing the time step there seems to alter the representation of the seasonal cycle.

This method allows the performing of only one baroclinic step instead of 8. After this first time step, the major velocity changes have already occurred. This was confirmed by the weak differences between the quasi-equilibrium solutions of two experiments, the first one using 8 baroclinic time steps for one scalar time step, the second using a 1 to 1 correspondence.

The numerical resolution of the equations governing the oceanic evolution is based on a finite-volume technique. In order to have a conservative discretisation, which is essential to avoid an artificial drift when long integrations are carried out, the exchanges between the grid boxes are performed by fluxes. The various variables are staggered following the B-grid of the classification of Arakawa (Mesinger and Arakawa, 1976). ($S, \rho, \theta, u, v, \eta, U, V, f$) are located at the centre of the level and (w, q^2, K_u, K_s) at the interfaces. On the horizontal plane ($\eta, S, \theta, \rho, w, q^2, K_s$) are at the "centre", whereas (U, V, u, v, K_u, f) are at the "corners" (Fig. 3). One classical problem of the B-grid is the development of a numerical checkerboard mode on the elevation. To limit the amplitude of this mode, a conservative filter on the elevation is applied (Killworth et al., 1991; Deleersnijder and Campin, 1995; Campin, 1997)

⁷ The discrete form of the equations is not presented here. See Campin (1997) for a complete description.

The spatial discretisations of the momentum equation and of the vertical terms of the equations for scalars are based on classical centered schemes, and so they are not presented in detail here (but see Campin, 1997). The horizontal advection of scalars is discretised in a more sophisticated way because it is a dominant term in the equations of evolution (6) and (7) and thus very important for the water-mass properties. Furthermore, it is a quite delicate term to represent. In CLIO (Campin, 1997), a hybrid scheme (e.g., Rood, 1987) is applied which is a combination of a upwind scheme and a centred scheme by means of the parameter α (upwinding rate). It works grossly as follows: for a value of α equal to zero, the scheme is identical to the centred scheme. As α increases, the scheme is more stable but also more diffuse. If α reaches 1, the upwind scheme is obtained. The numerical diffusion of the scheme is equivalent to a diffusivity of $\alpha|u|\Delta x/2$, where Δx is the grid spacing in the corresponding direction and u the velocity).

The parameter α is variable with both time and space and is determined in the way proposed by James (1986), modified by Campin (1997). α is chosen so that the scheme is equivalent to the Lax-Wendroff scheme in regions where gradients are weak but becomes closer to an upwind scheme where the gradients are stronger and more diffusion is needed to limit the numerical over or undershooting. For the extension of the scheme to more than one dimension, the fractional step method (see Campin, 1997) is used in which the equations are first integrated in a nearly 1-D mode along one direction (X) and then along the others (Y), the reverse (Y and then X) being applied in the next time step.

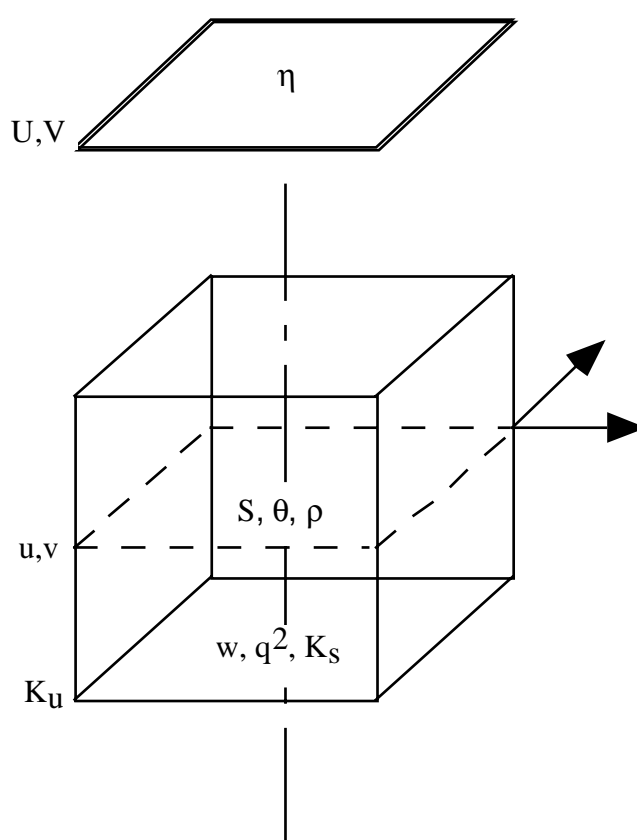


Fig.3 Location of the various variables on the model grid.

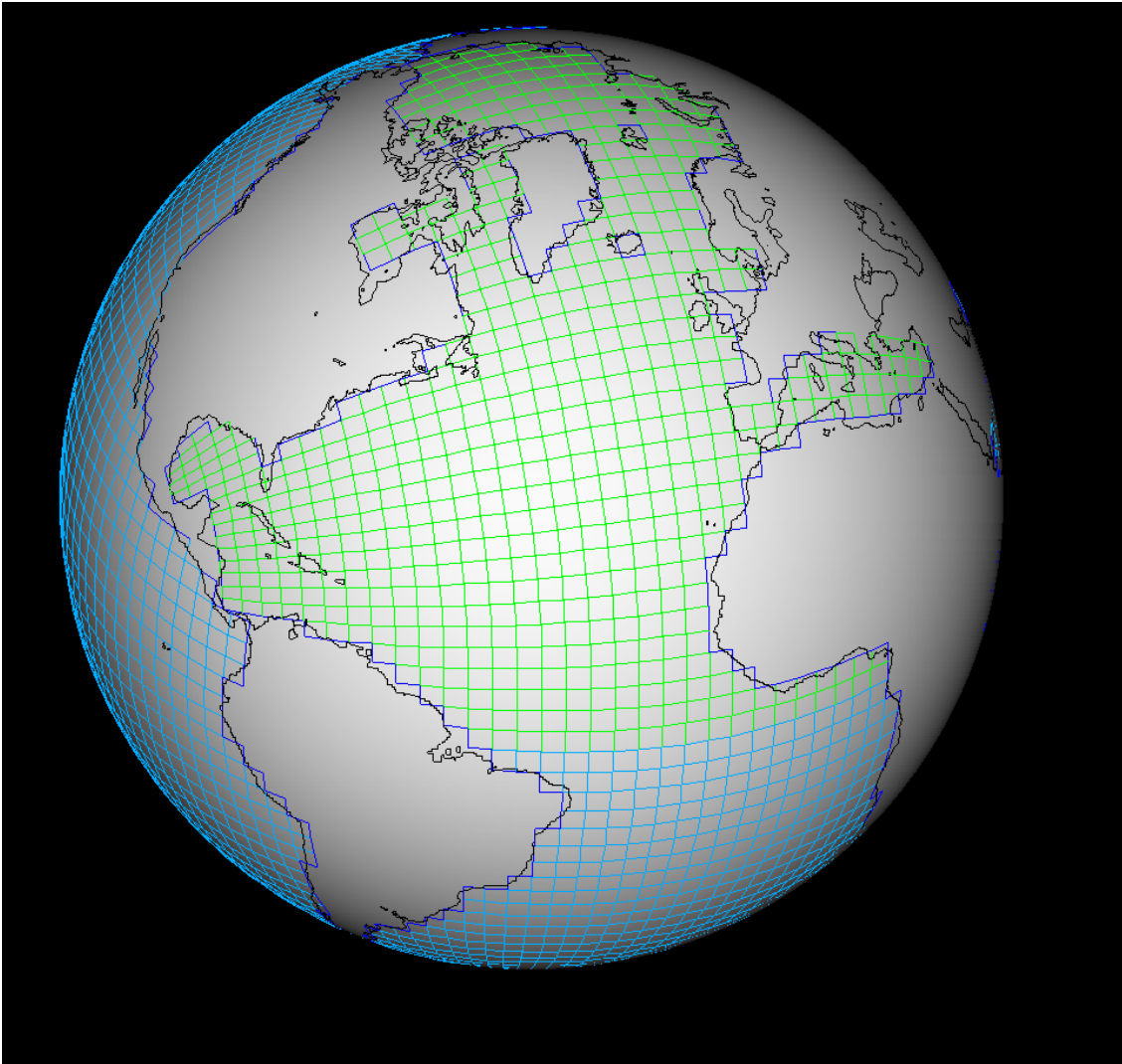


Fig.4 The horizontal grid in the coarse resolution version of the model. The view is centred on the Atlantic. The two spherical subgrids are connected in the Atlantic at the "geographical equator" (Figure from J.-M. Campin).

The most natural way to discretise equations on the Earth (which is supposed to be a perfect sphere) is to use spherical coordinates. However, in this kind of grid, there is a singularity at the poles. This does not cause any trouble at the South Pole since it is located well inside the continent, but it is not the case at the North Pole. The method used here to avoid this problem is to associate two spherical subgrids, for which the poles are not located in the oceanic domain covered by the grid (Fig. 4). The first one is based on classical longitude-latitude coordinates. It covers the Southern Ocean, the Pacific Ocean, the Indian Ocean and the South Atlantic. The second spherical subgrid has its poles located at the equator, the "north pole" in the Pacific (111°W) and the "south pole" in the Indian Ocean (69°E). The remaining parts of the ocean are represented on this "rotated" grid, i.e., the North Atlantic and the Arctic. The two subgrids are connected in the equatorial Atlantic where there is a correspondance between the meridians of the South Atlantic on one grid and the parallel of the other grid in the North Atlantic (Deleersnijder et al., 1993; Campin, 1997). The grid spacing on both grids is $3^{\circ}\times 3^{\circ}$ in the low-resolution version and $1.5^{\circ}\times 1.5^{\circ}$ in the high-resolution one. In the model, the two subgrids are considered as a single coordinate system using metric coefficients which are given by Deleersnijder et al. (1993) or Campin (1997).

Because of the grid system, the direct connection between the Pacific and the Arctic through the Bering Strait is not directly taken into account. To solve this problem, it has been chosen to parameterize the water flow through the Bering Strait as a linear function of the cross-strait sea-level difference in accordance with geostrophic control theory (Toulany and Garrett, 1984). For more details and for the role of the Bering Strait throughflow, see Campin(1997) and Goosse et al. (1997a).

Table 1. Depth and thickness of the vertical layers in the coarse resolution version.

Level (k)	Depth of the center (m)	Thickness of the level	Location of the bottom interface
20	5.00	10.00	10.00
19	15.98	11.96	21.96
18	29.17	14.42	36.38
17	45.20	17.64	54.02
16	64.96	21.88	75.90
15	89.75	27.70	103.60
14	121.52	35.84	139.44
13	163.28	47.68	187.12
12	219.86	65.48	252.60
11	299.26	93.38	345.98
10	415.07	138.18	484.16
9	588.88	209.44	693.60
8	850.19	313.18	1006.78
7	1225.11	436.66	1443.44
6	1717.90	548.92	1992.36
5	2307.36	630.00	2622.36
4	2963.25	581.78	3304.14
3	3661.11	713.94	4018.08
2	4385.22	734.28	4752.36
1	5126.18	747.64	5500.00

The vertical discretisation follows the simple so-called "z-coordinate" (Campin, 1997). This means that the depth of each level is fixed as well as the location of the interface between levels. The bottom of the ocean is considered as a succession of steps, at each point, the number of active levels being chosen to have the best correspondence between the model depth and the real ocean depth.

Table 2. Depth and thickness of the vertical layers in the high resolution version.

Level (k)	Depth of the center (m)	Thickness of the level	Location of the bottom interface
30	5.00	10.00	10.00
29	15.38	10.76	20.76
28	26.62	11.72	32.48
27	38.94	12.92	45.40
26	52.62	14.44	59.64
25	68.07	16.46	76.30
24	85.87	19.14	95.44
23	106.87	22.86	118.30
22	132.35	28.10	146.40
21	164.29	35.78	182.18
20	205.83	47.30	229.48
19	261.99	65.02	294.50
18	340.52	92.04	386.54
17	451.91	130.74	517.28
16	606.54	178.52	695.80
15	808.85	226.10	921.90
14	1054.05	264.30	1186.20
13	1331.64	290.88	1477.08
12	1631.22	308.28	1785.36
11	1945.16	319.60	2104.96
10	2268.53	327.14	2432.10
9	2598.26	332.32	2764.42
8	2932.40	335.96	3100.38
7	3269.70	338.64	3439.02
6	3609.71	340.62	3779.64
5	3950.71	342.14	4121.78
4	4293.44	343.32	4465.10
3	4637.23	344.26	4809.36
2	4981.86	345.00	5154.36
1	5327.18	345.64	5500.00

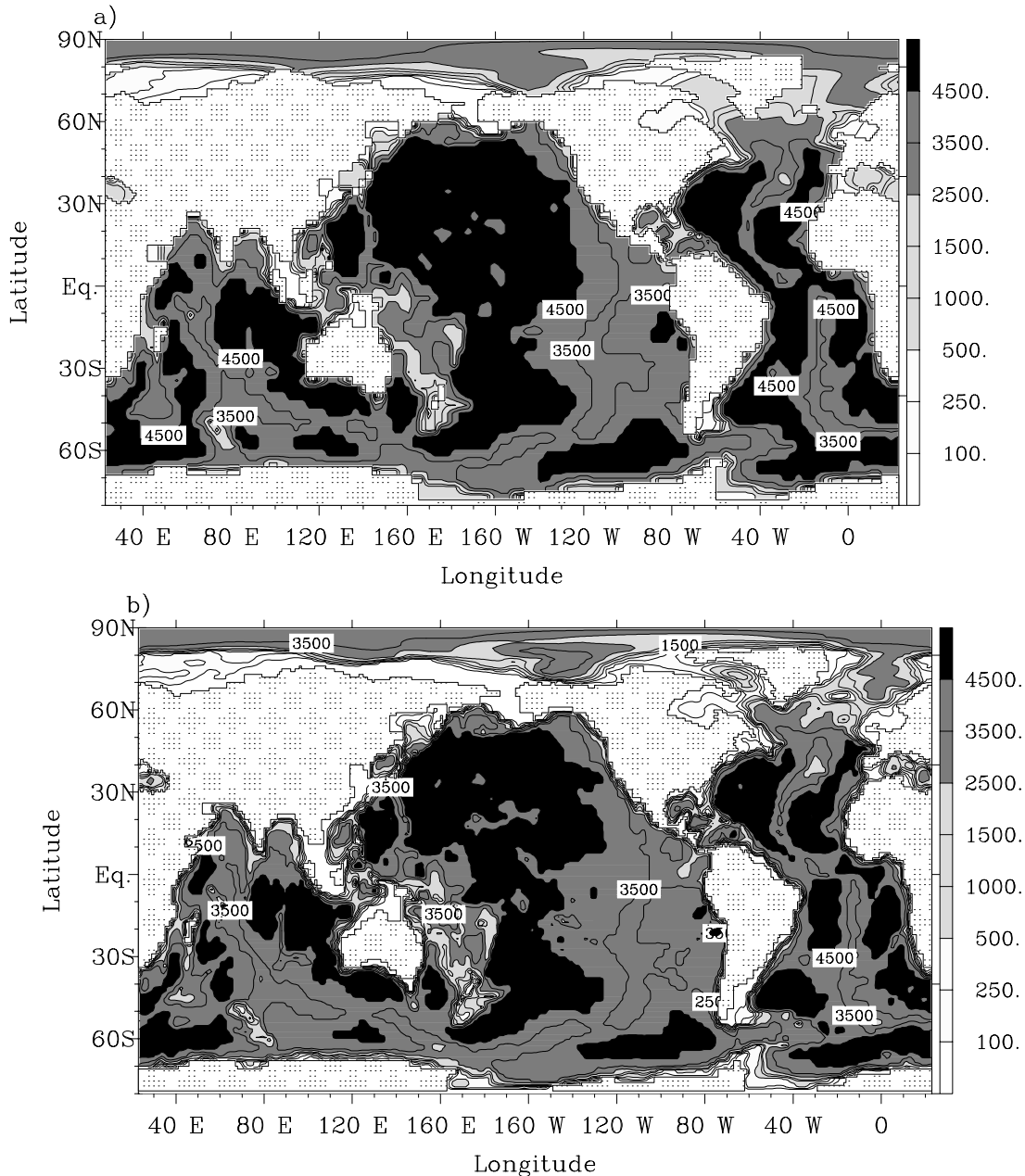


Fig.5. The bathymetry (m) of the world ocean as represented in the low (a) and high (b) resolution versions of the model.

It is necessary to have a relatively fine resolution close to the surface to obtain a good representation of the strong gradients that occur there. Furthermore, a correct description of the mixing in the upper ocean as well as the turbulence model also needs a fine grid. Deeper in the ocean, the time and space variations are smaller. As a consequence, a depth-varying vertical grid with fine resolution close to the surface and coarser resolution in the deep ocean seems to be adequate. In the low-resolution version, there are 20 levels ranging from 10 m at surface to a maximum of 750 m near the bottom (Table 1) while in the high-resolution one there are 30 levels ranging from 10 m at surface to a maximum of 350 m near the bottom (Table 2).

The bathymetry used in the model is based on the global topography given in 5x5 minutes by ETOPO 5 (1986). Each model grid cell is considered to be an oceanic point ("wet point") if the real oceanic volume associated with this box is greater than

40% (Campin, 1997). Some further modifications are needed to avoid isolated points where it is not possible to compute a velocity.

For the coarse resolution version, it has been necessary to modify some points in order to have a better representation of the important straits which allow exchanges between oceanic basins (Fig. 5.a). The major places where adaptations have been made are (Campin, 1997): the Indonesian Archipelago, the Canadian Archipelago, the regions southward of Iceland and between Australia and New-Zealand, the Mediterranean Sea and the Japan Sea. The sill depth of the passages between Greenland, Iceland and Scotland has been increased to 1440 m (the observed maximum depth of these straits being about 900 m). This is a classical method to increase the exchanges between the GIN Sea (Greenland, Iceland and Norwegian seas) and the North Atlantic in coarse-resolution models (Roberts et al., 1996; Campin, 1997). The only differences between our representation of the bathymetry and that of Campin (1997)⁸ are the introduction of an island representing Spitzbergen and the opening of a passage through the Canadian Archipelago to allow direct exchanges between the Arctic and Baffin Bay (Goosse et al., 1997c). Several adaptations of the original bathymetry have also been made in the high resolution version (Fig. 5.b). The total ocean surface is $3.62 \times 10^{14} \text{ m}^2$ and $3.61 \times 10^{14} \text{ m}^2$ for the low and high resolution versions of the model, respectively (to be compared with $3.61 \times 10^{14} \text{ m}^2$ for the real ocean (Gill, 1982)). The volume is $1.40 \times 10^{18} \text{ m}^3$ and $1.37 \times 10^{18} \text{ m}^3$ for the low and high resolution versions of the model, respectively ($1.37 \times 10^{18} \text{ m}^3$ according to Trenberth, 1992).

3. The sea-ice component

The physical processes governing the evolution of sea ice can be conceptually divided into two parts. The first one concerns the thermodynamic growth or decay of the ice (sub-sections 3.1 and 3.2), which can be considered to depend only on the vertical response of the ice layer to the exchanges with the atmosphere and the ocean⁹. The horizontal thermodynamical processes, such as the horizontal heat conduction through ice, can be safely neglected because of the much larger horizontal scales. On the other hand, the ice dynamics and transport (sub-sections 3.3 and 3.4) can be considered at large scale as horizontal processes, the ice velocity being homogenous from the bottom to the top of the ice. This distinction between thermodynamics and dynamics is purely formal since they are intrinsically coupled. The ice growth is a function of the ice thickness and concentration (the smaller the ice thickness and concentration, the faster the ice growth and decay (Maykut, 1982)) which in turn depends strongly on the advection pattern. Conversely, the motion of sea ice is to a great extent affected by the ice-thickness distribution which roughly controls the amount of stress the ice can sustain (Hibler, 1979).

3.1. Vertical growth and decay

The representation of the vertical growth and decay of sea ice is based on the model of Fichefet and Gaspar (1988) which is an improved version of the 3-layer model

⁸ Campin(1997) used only 15 levels. The correspondence between the 20- and 15-level discretisations has been realised so as to change the local oceanic depth as little as possible.

⁹ It could seem strange that the lateral growth or decay of sea ice is described as a vertical process, but it is mainly a function of the vertical fluxes from the atmosphere and the ocean as explained in sub-section 3.2.

of Semtner (1976) (Morales Maqueda, 1995; Fichefet and Morales Maqueda 1997). Within the ice-covered portion of each grid cell¹⁰, sea ice is considered as a homogenous slab of ice on which a snow layer can be present as a consequence of snow precipitation. The evolution of temperature inside the snow-ice system is governed by the one-dimensional heat-diffusion equation :

$$\rho_c c_{pc} \frac{\partial T_c}{\partial t} = G(h_e) k_c \frac{\partial^2 T_c}{\partial z^2} , \quad (41)$$

where ρ_c , c_{pc} , and k_c are the density, the specific heat and thermal conductivity, respectively (their values are given in table 3). T_c is the temperature. The subscript c stands either for ice (i) or snow (s). $G(h_e)$ is a correction factor which represents the effects of the subgrid-scale snow and ice-thicknesses distributions on the conductive heat flux (Mellor and Kantha, 1989). It is well known that the thin ice experiences much stronger fluxes than thicker ice and, even if it represents only a small fraction of the ice cover, it can account for the major part of the conductive flux (Maykut, 1982). Mellor and Kantha (1989) use a constant value for G , determined empirically from observed ice-thickness distribution. Here, $G(h_e)$ varies both with time and with space. It is diagnosed by assuming that the snow and ice thicknesses are uniformly distributed on the ice-covered part of the grid cell between zero and twice their mean value. Ignoring the heat capacity of the system, one obtains (Morales Maqueda, 1995; Fichefet and Morales Maqueda 1997):

$$G(h_e) = 1 + \frac{1}{2} \ln \left(\frac{2 h_e}{e \varepsilon} \right) . \quad (42)$$

e is the base of the natural logarithm. h_e is an effective thickness defined as

$$h_e = \frac{k_s k_i}{k_s + k_i} \left(\frac{h_s}{k_s} + \frac{h_i}{k_i} \right) , \quad (43)$$

where h_s and h_i are the thicknesses of snow or ice, respectively. The threshold thickness ε determines the limit of validity of Eq. (42). For $h_e < e\varepsilon/2$, $G(h_e)$ is taken equal to 1. In practice, the value of G is generally between 1.5 and 2 (Mellor and Kantha, 1989; Fichefet and Morales Maqueda, 1997).

Numerically, two temperatures are computed inside the ice and one temperature inside the snow. The Eq. (41) is solved using an implicit method in order to prevent numerical instabilities for thin ice slabs (Morales Maqueda, 1995). The time step (dtb) is set identical to dts, the time step for the scalars in the ocean.

The surface temperature is determined by considering the budget of a thin layer of thickness h_{su} at the top surface :

$$h_{su} (\rho c_p)_{su} \frac{\partial T_{su}}{\partial t} = (1 - i_0) F_{sw} + F_{lw} - \varepsilon_{su} \sigma T_{su}^4 + F_h + F_{le} + F_{cs} , \quad (44)$$

where su refers to the top surface (snow or ice). F_{sw} is the net shortwave radiation (albedo effect included), i_0 is the fraction of net shortwave radiation which is not

¹⁰See section 3.2. for a definition of the ice concentration, A

absorbed in the thin surface layer and penetrates inside the ice cover. F_{lw} is the downward longwave radiation absorbed at surface, ϵ_{su} is the surface emissivity and σ is the Stefan-Boltzman constant. F_h and F_{le} are the turbulent fluxes of sensible and latent heat, respectively (see also section 5). F_{cs} is the conductive heat flux from below. The convention used in Eq. (44) is that a flux toward the surface is taken positive, while one away from the surface is negative. i_0 is set equal to 0 for snow-covered ice (Maykut and Untersteiner, 1971). When ice is free of snow, i_0 is parameterized as (Ebert and Curry, 1993) :

$$i_0 = 0.18(1 - c_{ld}) + 0.35 c_{ld} , \quad (45)$$

where c_{ld} is the fractional cloud amount.

If the heat balance (44) requires that the surface temperature is above the melting point (T_{fsu}), T_{su} is held at this point and the excess of energy is balanced by melting snow or ice¹¹.

The thickness of the surface layer (h_{su}) is usually taken equal to zero which means that the heat capacity of the surface layer is negligible. The evolution of the heat content of this layer is indeed a very small element of the budget which does not affect the results. However, since it has proved to help to stabilise the system when coupled to an atmospheric model (H. Grenier, personal communication, 1995), a small, but non-zero, value has been kept here.

At the bottom of the ice slab, any imbalance between the conductive heat flux within the ice F_{cb} and the heat flux from the ocean F_w is balanced by accretion or ablation of ice:

$$\frac{\partial h_i}{\partial t} = \frac{F_{cb} - F_w}{L_i} , \quad (46)$$

where L_i is the volumetric heat of fusion of ice.

The part of solar radiation absorbed inside the ice, assuming an exponential absorption within the ice (Grenfell and Maykut, 1977), is given by :

$$F_{si} = i_0(1 - \alpha_{su}) \left[1 - e^{-1.5(h_i - h_{su})} \right] F_{sw} . \quad (47)$$

α_{su} is the surface albedo (see sub-section 5.1). In summer, this energy is used to increase the volume of brine pockets (very salty water which is incorporated inside the ice when seawater freezes). This latent heat is released in autumn through the refreezing of brine pockets. This mechanism of "brine damping" is parameterized following the approach of Semtner (1976) wherein F_{si} is stored in a heat reservoir that represents internal meltwater. Energy from this reservoir is used to keep the temperature of the upper ice layer from dropping below the freezing point before the reservoir is empty.

When the load of snow is large enough to depress the boundary of the snow layer under the water level, seawater is assumed to infiltrate the submerged snow and to freeze there forming snow ice. The change of ice thickness after snow-ice formation is

¹¹To be comprehensive, it must be added that a small mass variation at the surface also occurs because of the sublimation associated with the latent heat flux F_{le} .

such that the interface between snow and ice is located at the same height as the ocean surface. It is given by (Fichefet and Morales Maqueda, 1999):

$$(\Delta h_i)_{si} = -\frac{(\Delta h_s)_{si}}{\beta_{si}} = \frac{\rho_s h_s - (\rho_0 - \rho_i) h_i}{\beta_{si} \rho_s + \rho_0 - \rho_i} . \quad (48)$$

β_{si} is an empirical parameter taking into account the compaction of the soaked snow ($\beta_{si}=1.0$). In this parameterization, the mass of snow ice newly formed $(\rho_i \Delta h_i)_{si}$ is constituted of a contribution from the snow $(\rho_s \Delta h_i)_{si}$ and a contribution from the infiltrated seawater $(\rho_i - \beta_{si} \rho_s) (\Delta h_i)_{si}$. The latent heat and brine release occurring during the freezing of the water component are transferred to the ocean.

3.2 Lateral growth and decay of the ice

The floes within the ice pack are separated by zones of open water: leads and polynyas. Leads are linear features appearing as a result of divergent ice motion that pulls the ice apart. They are generally narrow (ten to hundreds of meters wide) and long (kilometres to tens of kilometres long) (Gow and Tucker, 1990). Polynyas (from "lake" in Russian) are rectangular or more or less elliptically shaped, with a larger characteristic length. These areas of open water are very important, even if they cover only a small fraction of the surface, since they allow direct exchanges between the atmosphere and ocean and thus much stronger fluxes than when ice is present (see, for example, Smith et al. (1990) for an overview of the processes related to leads and polynyas). This fraction of open water is represented in the model by the introduction of the variable A , the ice concentration, which is the percentage of each cell which is covered by ice ($0 \leq A \leq 1$). This distinction between ice and open water can be considered as a very crude simplification of the distribution of the ice between different ice-thickness categories developed by Thorndike et al. (1975).

The thermodynamic variations of A are function of the heat budget of the open water B_l (expressed in W/m^2) which is computed in the same way as the heat flux toward the ocean (see section 5). If B_l is negative ice is formed in the open water and A tends to decrease following the law (Morales Maqueda, 1995; Fichefet and Morales Maqueda 1997):

$$\left(\frac{\partial A}{\partial t} \right)_{acc} = -\Phi(A) \frac{(1-A) B_l}{L_i h_0} . \quad (49)$$

$[(1-A) B_l / L_i]$ is the amount of ice created in the leads. $\Phi(A)$ is a monotonic, non-increasing function such that $\Phi(0) = 1$ and $\Phi(1) = 0$. h_0 is a characteristic thickness of the ice created in the lead. One possible interpretation of Eq. (49) is that the ice created in the lead has a thickness of $h_0 / \Phi(A)$, which increases with A . When no ice is present, the open water tends to be covered by ice with a relatively low thickness h_0 . When the concentration increases, the new ice tends to have a much higher thickness, because, for example, of piling of the ice against the wall of the existing floes (Bauer and Martin, 1983), or of dynamic effects which tend to compress the less resistant new ice and increase its thickness (Parameter and Coon, 1972; Hopkins et al., 1991). Another interpretation of Eq. (49) is to consider that the ice formed in the lead has always a thickness h_0 , but only a fraction $\Phi(A)$ of the ice formed contributes to the increase of the ice concentration. The remaining part is rather assumed to lead to an increase in the

thickness of the pre-existing ice, through, for example, the transport of frazil ice formed in the lead towards the ice covered region. This parameterization is somewhat similar to that of Häkkinen and Mellor (1992) in which h_0 is proportional to h_i . The following form for $\Phi(A)$ has been chosen (Morales Maqueda, 1995; Fichefet and Morales Maqueda, 1997):

$$\Phi(A) = (1 - A^2)^{1/2}. \quad (50)$$

Whenever lateral accretion of ice occurs, the thickness of newly formed ice is averaged with that of pre-existing ice to obtain a single value and snow is distributed over the new ice-covered area.

Table 3. Standard numerical values of the constants and parameters used in the sea ice model (adapted from Fichefet and Morales Maqueda, 1997)

Symbol	Definition	Value
c_{pi}	specific heat of sea ice	2093 J Kg ⁻¹ K ⁻¹
c_{ps}	specific heat of snow	2093 J Kg ⁻¹ K ⁻¹
C	ice strength parameter	20
D	horizontal diffusivity	300 m ² s ⁻¹
e_c	eccentricity of the yield curve	2
ε	threshold thickness for the computation of $G(h_e)$	0.1 m
ε_{su}	emissivity of snow or ice	0.97
h_0	thickness of newly formed ice in leads	0.3 m
h_{su}	thickness of the surface layer used in the computation of the surface temperature	0.1 m
k_i	thermal conductivity of sea ice	2.0344 W m ⁻¹ K ⁻¹
k_s	thermal conductivity of sea snow	0.21 W m ⁻¹ K ⁻¹
L_i	volumetric latent heat of fusion of sea ice	300.330 x 10 ⁶ J m ⁻³
L_s	volumetric latent heat of fusion of snow	110.121 x 10 ⁶ J m ⁻³
$\dot{\varepsilon}_0$	threshold use in ice dynamics	2 x 10 ⁻⁸ s ⁻¹
P^*	ice strength parameter	15000 N m ⁻²
ρ_i	density of sea ice	900 kg m ⁻³
ρ_s	density of snow	330 kg m ⁻³
T_{fi}	melting point of sea ice	273.05 K
T_{fs}	melting point of snow	273.15 K

In summer, the lateral melting seems to be rather negligible, the thermodynamic decrease of ice concentration being, for the most part, caused by the total vertical melting of thin ice. The parameterization of this effect is based on the work of Häkkinen and Mellor (1990). When B_l is positive, it is supposed that the entire heat gain in leads contributes to basal melting¹² through F_w . If one assumes that the ice is uniformly distributed in thickness between 0 and $2h_i$ over the ice covered portion of the grid cell and that the melting rate is independent of the local ice thickness, the vertical ice melting necessary implies a reduction in ice concentration given by (Fichefet and Morales Maqueda 1997; Morales Maqueda, 1995):

¹² Assuming that a small part of B_l is used directly for lateral melting does not change significantly the results when using the parameterization (II.48).

$$\left(\frac{\partial A}{\partial t}\right)_{abl} = -\frac{A}{2h_i} \Gamma \left[-\left(\frac{\partial h_i}{\partial t}\right) \right], \quad (51)$$

where Γ is the Heaviside function.

3.3 Ice dynamics

When studying the motion of sea ice at length scales of the order of tens of kilometres and larger, the ice can be considered as a two-dimensional continuum. Its momentum balance can be expressed as :

$$m \frac{\partial \mathbf{u}_i}{\partial t} = \boldsymbol{\tau}_{ai} + \boldsymbol{\tau}_{wi} - m f \mathbf{e}_z \times \mathbf{u}_i - mg \nabla \eta + \mathbf{F}, \quad (52)$$

where m is the mass of snow and ice per unit area, \mathbf{u}_i is the ice velocity. $\boldsymbol{\tau}_{ai}$ and $\boldsymbol{\tau}_{wi}$ are the forces per unit area from the air and water, respectively. \mathbf{F} is the force per unit area due to internal interactions. f , \mathbf{e}_z , g , and η are respectively the Coriolis parameter, a unit vector pointing upward, the gravitational acceleration, and the sea-surface elevation, as already defined in section 2.

In Eq. (52), the advection of momentum has been neglected since scale analysis has shown that it is much smaller than other forces acting on the pack (e.g., Thorndike, 1986a). The first two terms of the right-hand side represents the exchanges of momentum between atmosphere or ocean and sea ice. The third term is the Coriolis force. The fourth one is the force acting on the ice due to pressure gradients associated with the tilt of the ocean surface (see Hibler, 1979, 1986 or Morales Maqueda, 1997 for more details.)

The internal force \mathbf{F} can be written in term of the divergence of the two-dimensional stress tensor, $\mathbf{F} = \nabla \cdot \boldsymbol{\sigma}$. To close the system, it is necessary to specify a stress-strain relationship, also called "constitutive law". This law must reproduce the most important characteristics of the ice behaviour at large scale (Hibler, 1979) : (1) sea ice seems on average isotropic; (2) tensile strength is very low; (3) strength under compression can be very large; (4) stress is nearly independent of the strain rate $\dot{\boldsymbol{\epsilon}}$ (plastic flow).

To match these characteristics, Hibler (1979) has proposed a viscous-plastic constitutive law, in which the non-linear viscosities are chosen in such a way that the ice behaves as a rigid plastic medium for normal to high deformation rates and as a viscous fluid for very small deformation rates:

$$\boldsymbol{\sigma} = 2\mu\dot{\boldsymbol{\epsilon}} + \left[(\zeta - \mu)\mathbf{T}(\dot{\boldsymbol{\epsilon}}) - \frac{P}{2} \right] \mathbf{I}, \quad (53)$$

where μ and ζ are the non-linear bulk and shear viscosities, respectively, $\mathbf{T}(\dot{\boldsymbol{\epsilon}})$ is the trace of the strain-rate tensor, P is the ice strength, and \mathbf{I} is the two-dimensional unity tensor. The viscosities are given by :

$$\zeta = \frac{P}{2\Delta}, \quad (54)$$

$$\mu = \frac{\zeta}{e_c^2}, \quad (55)$$

with

$$\Delta = \max \left\{ \dot{\epsilon}_0, \left[\mathbf{T}^2(\dot{\epsilon}) \left(1 + \frac{1}{e_c^2} \right) - D(\dot{\epsilon}) \frac{4}{e_c^2} \right]^{1/2} \right\}. \quad (56)$$

$D(\dot{\epsilon})$ is the determinant of the strain-rate tensor. Eqs. (53) to (56) correspond to an elliptical yield curve with e_c being the ratio of the principal axes of the ellipse (eccentricity). $\dot{\epsilon}_0$ is a parameter termed "creep limit"

Following Hibler (1979), the ice strength is parameterized as :

$$P = P^* A h_i e^{-C(1-A)}, \quad (57)$$

where P^* and c are empirical constants. Eq. (57) means that ice strength decreases strongly if the ice concentration decreases and increases slowly (linearly) with ice thickness.

The ice momentum equation is solved on the same horizontal grid as the ocean model. The ice thickness, concentration and mass are located at the "centre" of the grid cell (same location as θ , S , η , see Fig. 2) and the velocity at the corners. The resolution mainly follows the method proposed by Hibler (1979) (see Morales Maqueda, 1995). Firstly, the velocity is computed at fractional time step $(k+1/2)\Delta t_d$ from the velocity at time step $k\Delta t_d$ by using a linearisation of the equations. The non-linear terms are evaluated from the new velocities. Secondly, the solution at $(k+1)\Delta t_d$ is obtained, the non-linear term being centred at $(k+1/2)\Delta t_d$. At each of these two time steps, the linear equations are solved by an implicit method, applying an underrelaxation technique. The time step Δt_d is set equal to 24 hours.

3.4. Horizontal transport

The local changes of any variables, due to the large-scale transport by ice motion and to the processes described in section 3.1 and 3.2, can be expressed by the general conservation law:

$$\frac{\partial \psi}{\partial t} = -\nabla \cdot (\mathbf{u}_i \psi) + D \nabla^2 \psi + S_\psi, \quad (58)$$

where ψ represents the physical variables that are transported in the model : the snow volume per unit area Ah_s , the ice volume per unit area Ah_i , the ice concentration, the snow and ice sensible heat contents per unit area AQ_s and AQ_i (with $Q_s = \rho_s c_{ps} \int_0^{h_s} T_s(z) dz$; $Q_i = \rho_i c_{pi} \int_0^{h_i} T_i(z) dz$) and the latent heat content in the brine reservoir. S_ψ is the rate of change of ψ due to thermodynamic effects and D is a horizontal diffusivity. The diffusion term is used to damp non-linear instabilities arising from the coupling between ice dynamics and transport. The diffusivity used here is much higher than the one that could be deduced from the random motions in the ice field

(Thorndike, 1986b). It takes a constant value inside the pack and is set equal to zero at the ice edge.

The advection is computed numerically by making use of the scheme of Prather (1986) which is based on the conservation of second-order moments. It is weakly diffusive and allows to avoid unphysical negative values.

4. Coupling the oceanic and sea-ice components

The ocean and sea ice exchange momentum, heat, and mass. Only the ice bottom interface is considered here. The effects of leads are only taken into account through their influence on the lateral growth or decay of sea ice (sub-section 3.2). Furthermore, as in nearly all ice-ocean models, the vertical extent of the top oceanic grid box is not affected by the presence of ice ("ice can be viewed as resting on the top of the ocean"). Taking explicitly into account the modifications of the surface grid box as a function of the ice draft would strongly complicate the treatment without significant advantage.

The parameterization of the various fluxes at the interface depends strongly on the structure of the boundary layer under ice. For rough surfaces such as sea ice, the boundary layer can be conceptually divided into various sublayers (e.g., McPhee et al., 1987) :

- a thin *molecular sublayer* in which viscous effects dominate;
- a *transition region* where both turbulent and viscous forces can be important;
- a *fully turbulent region* where the viscous effects are negligible.

The transition sublayer is classically thought to have a thickness of the order of the size of the dominant roughness elements (generally a few centimeters to tens of centimeters), the thickness of the molecular (or viscous) layer being much smaller

The *fully turbulent layer* is generally decomposed into two parts. The *surface sublayer*, where the flow is unidirectional. Its extension is estimated to be of the order of $0.03u_* / f$ (Tennekes, 1973) which is about 2-5 m for typical under-ice conditions. u_{*io} is the friction velocity defined as $|\tau_{iw}| = \rho_0 u_{*io} u_{*io}$, τ_{iw} being the ice-ocean stress. Below this layer, the Coriolis force becomes important and the flow begins to veer significantly. This region is called the *Ekman layer* (or *outer layer*).

4.1. Exchange of momentum

Sea ice is generally considered to be hydraulically rough (McPhee et al., 1987; Shirasawa and Ingram, 1991). The roughness Reynolds number ($Re_* = u_* z_0 / \nu$, where z_0 is the roughness parameter or roughness length and ν is the water kinematic viscosity $\nu = 1.8 \times 10^{-6} \text{ m}^2/\text{s}$) typically ranges from 10^2 to 10^4 , while laboratory experiments have shown that the flow is rough for values greater than 10 and even below (McPhee et al., 1987; Shirasawa and Ingram, 1991). For such surfaces, the molecular viscosity plays no role in determining the mean velocity profile below the transition layer (McPhee et al., 1987). As a consequence, it is only necessary to take into account the surface and Ekman layers for computing the ice-ocean stress which results from surface integral of the pressure force acting on under-ice protrusions (Mellor et al., 1986). It must be stressed that the coefficients used in the parameterization based on this hypothesis have to be deduced from observations made well outside the transition sublayer in order to include the effect of all the protrusions or ice keels (McPhee et al., 1987; Shirasawa and Ingram, 1991).

Numerous observations have shown that in the surface layer, the stress is nearly constant while the velocity strongly changes, keeping the same direction (e.g., Hunkins, 1975; McPhee, 1986; McPhee et al., 1987). If the surface layer is neutrally buoyant (no density variation), this leads to the well-known logarithmic profile (e.g., McPhee, 1986) :

$$|\mathbf{u}(z) - \mathbf{u}_i| = \frac{u_*}{k} \ln \frac{|z|}{z_0}, \quad (59)$$

where k is the von Karman constant already defined ($k=0.4$). When deducing Eq. (59), it has been assumed that the viscosity can be given by the classical expression $K_u = u_* k z$, u_* being the velocity scale and kz the length scale characteristic of the turbulent motion (see sub-section 3.2).

Eq. (59) can be used to compute the surface stress :

$$|\tau_{iw}| = \rho_0 u_*^2 = \frac{\rho_0 k^2}{\left(\ln \frac{|z|}{z_0}\right)^2} |\mathbf{u}_i - \mathbf{u}(z)|^2. \quad (60)$$

The drag coefficient c_w is often introduced in Eq. (60):

$$c_w = \frac{k^2}{\left(\ln \frac{|z|}{z_0}\right)^2}. \quad (61)$$

Finally, the expression for τ_{iw} in vectorial form reads:

$$\tau_{iw} = \rho_0 c_w |\mathbf{u}_i - \mathbf{u}(z)| (\mathbf{u}_i - \mathbf{u}(z)), \quad (62)$$

where the convention adopted is that τ_{iw} is the stress of the ice on the water ($\tau_{iw} = -\tau_{wi}$; τ_{wi} , defined in sub-section 3.3, is the stress of the ocean on the ice).

To apply Eq. (62) as a boundary condition in a model, it is necessary to compute one velocity point in the surface layer in order to provide $\mathbf{u}(z)$. In the standard version of CLIO, the first velocity point is located at 5 m depth below the surface. This depth is in the range of theoretically estimated surface-layer (see above) and, according to observations (Hunkins, 1975; McPhee et al., 1987), the veering is generally low there. As a consequence, the ice-ocean stress is computed by Eq. (62) in this study without any correction.

The value of z_0 estimated from observations varies from less than 0.5 cm to more than 10 cm (see Shirasawa and Ingram, 1991 for a review of various estimates)¹³. Here, a value of z_0 equal 2 cm) is used (this corresponds to a c_w at 5m equal to 5×10^{-3}) which is in the range of observed values and gives satisfactory results in the model.

4.2. Exchange of heat

¹³ It must be stressed that z_0 is included in a logarithm to compute c_w , so the variations of c_w are much lower than those of z_0 . For example, c_w at 5 m varies from 4×10^{-3} to 10×10^{-3} if z_0 ranges from 1 to 10 cm.

There is no correspondence for heat of the pressure force on the under-ice protrusions and any flux of heat must be ultimately transferred through the viscous sublayer. It is obviously impossible to resolve this layer in a three-dimensional model, so its effect must be parameterized somehow. McPhee (1992) has proposed to express the heat flux as a simple function of the temperature of the ocean and of the turbulent mixing :

$$F_w = \rho_o c_{pw} c_h u_{*io} (T_1 - T_{Freez}) , \quad (63)$$

where T_1 is the mixed layer temperature and T_{Freez} is the freezing point of mixed layer , a function of the salinity S_1 determined in this study from Doronin and Khesisin's (1977) formula :

$$T_{Freez}(S_1) = 273.15 - (3.0 + 52.75 S_1 + 0.04 S_1^2 + 0.0004 S_1^3) \times 10^{-3} . \quad (64)$$

The coefficient c_h has been evaluated over a wide range of conditions and its value is surprisingly uniform ($c_h \sim 0.006$) (McPhee, 1992). c_h depends probably on the characteristics of the viscous sublayer as h_{ts} and not much on z_0 . Comparison with observations has shown that Eq. (60) performs as well as much more complex parameterizations. Therefore, this formulation has been chosen to calculate the ice-ocean heat flux in CLIO. A lower and an upper bound have been imposed on u_{*io} ($10^{-3} < u_* < 20/(dts c_h)$) to avoid too small values of the flux and to limit the maximum heat extracted during one time step (dts) by the total heat stored in the top 20 m (top 2 oceanic levels). Note that these values are rarely met. For example, the upper bound of u_* corresponds to about 4×10^{-2} m/s or a difference of velocity between the ocean and the ice of 55 cm/s.

4.3. Exchange of mass

Nearly no salt can be incorporated in the ice crystal lattice, but as the freezing process can be quite rapid, some salt can be trapped inside the ice during ice formation (brine pockets) (see Weeks and Ackley, 1986 or Gow and Tucker, 1990 for more details). Afterwards, the amount of salt in the ice has a tendency to decrease mainly as a result of gravity drainage (the heaviest brine moves toward the bottom and then to the ocean) and flushing (in spring and summer, surface meltwater percolates through the ice, diluting and entraining salt downward) (Weeks and Ackley, 1986; Gow and Tucker, 1990). This results in old ice generally much less salty than young ice, with values less than 4 ‰ for multyear ice, between 4 ‰ and 10 ‰ for first year ice and up to 15 ‰ for newly formed ice. These elements indicate that a careful description of the evolution of the salt inside the ice is necessary if one wants to have a precise and complete representation of the exchanges of salt between sea ice and ocean. However, this is quite a hard problem which needs a relatively high vertical resolution in the ice (Cox and Weeks, 1988) or an adequate representation of the processes responsible for salt rejections. Furthermore, the effect of ice dynamics on salt distribution must also be taken into account. A simpler solution has been chosen here, i.e., assuming a constant value for the sea ice salinity as it is done in nearly all the large-scale modelling studies ($S_{ice} = 4$ ‰). The major error introduced by this assumption should occur immediately after ice formation where strong time variations of the salinity are present. Consider an ice cover with an average thickness of 25 cm, a minimum threshold below which our simple ice distribution is not valid. The regression line proposed by Cox and Weeks

(1974) provides an average salinity of about 10 ‰. This means that more than 2/3 of the salt contained in the water has already been rejected and the ice salinity will continue to decrease. So, the approximation of S_{ice} as a constant seems to be reasonably valid, at least at large scale.

In the model there is two ways to represent the freshwater flux at the ocean surface: it is modelled as an equivalent salt flux or as a realistic freshwater flux (see sub-section 5.2). In the first version, the effects of mass exchanges between ice and ocean is included in a salt flux :

$$F_{salt} = S_{oce} \left(\frac{\partial m_s}{\partial t} \right)_{ab} + (S_{oce} - S_{ice}) \left(\frac{\partial m_i}{\partial t} \right)_{acc-abl} + (S_{oce} - S_{ice}) \left(\frac{\partial m_s}{\partial t} + \frac{\partial m_i}{\partial t} \right)_{si} + S_{ice} \left(\frac{\partial m_s}{\partial t} \right)_{si} \quad (65)$$

where S_{oce} is a reference salinity in the ocean (see sub-section 5.2), and m_s and m_i are the mass of snow and ice per unit area, respectively. The first term on the right-hand side of Eq. (65) simulates the freshwater flux to the ocean due to snow melting by a negative salt flux. The second one is associated with ice formation and melting. The third and fourth ones come from snow-ice formation. The third one represents the salt rejection that occurs because of the freezing of the water that infiltrates the submerged snow, whereas the fourth one corresponds to the salt needed to bring the snow to the adequate salinity (Fichefet and Morales Maqueda, 1997).

When using a more realistic freshwater flux representation, salt and freshwater transfers at the ice base require a special attention. Ice formation takes freshwater and salt out of the ocean, whereas both are released during ice melting. Because of the hydrostatic equilibrium, ice melting and formation do not induce a displacement of the sea-surface level. Therefore, the freshwater and salt exchanges at the ice base have to be maintained as an equivalent salt flux which only takes into account the dilution effect.

Snow precipitation over the ice floe is part of the hydrological cycle. Its ablation and its transformation into snow ice should be parameterised as a freshwater flux towards the ocean. Otherwise snow-ice formation will induce a sink of freshwater for the climate system and its melting will decrease the total oceanic salt content. Therefore, salt and freshwater fluxes at the ice base are defined as follows

$$F_{salt} = (S_{oce} - S_{ice}) \frac{\partial m_i}{\partial t}, \quad (66)$$

$$F_{snow} = -\frac{1}{\rho_s} \left(\frac{\partial m_s}{\partial t} \right)_{abl+si}, \quad (67)$$

where F_{snow} is a positive downward freshwater flux.

5. Boundary conditions and surface forcing

5.1. Surface flux of heat

The flux of heat at the ice and ocean surfaces are derived from semi-empirical (or bulk) formulae which relate the flux to the properties of the surface and of the lower atmosphere. Quite a lot of parameterizations have been proposed which can give

significantly different results. It has been possible to reject some parameterizations thanks to the comparison with observations or with the results of more sophisticated models (e.g. Simpson and Paulson, 1979; Fung et al., 1984; Dobson and Smith, 1988; Katsaros, 1990 for radiative fluxes; Blanc 1985, 1987 for turbulent fluxes; see also Simonsen and Haugan, 1996). However, these tests do not allow to find one parameterization which gives the best result in every circumstance. Therefore, some relatively arbitrary choice must be made. In the present study, we follow the work of Oberhuber (1988) who has selected widely accepted parameterizations which have a global validity. Furthermore, slight modifications to the original parameterizations have been introduced (Oberhuber, 1988) in order to approach a global heat balance and to have reasonable heat transport in the ocean. A similar method was applied more recently by Da Silva et al. (1995) to avoid a systematic global ocean warming in their results.

The turbulent fluxes of sensible and latent heat are computed from the classical bulk formulas:

$$F_h = \rho_a c_{pa} c_{sh} V_a (T_a - T_{su}) , \quad (68)$$

$$F_{le} = \rho_a L_w c_{le} V_a (q_a - q_{su}) . \quad (69)$$

ρ_a is the air density (computed from the state equation of state of the perfect gases), c_{pa} is the specific heat of the air ($1005 \text{ J Kg}^{-1} \text{ K}^{-1}$), V_a and T_a are the air velocity and temperature close to the surface (assumed to be 10 m), respectively, and T_{su} is the surface temperature (snow, ice, or ocean). L_w is the latent heat of evaporation ($L_{we}=2.5 \times 10^6$

J Kg^{-1}) or of sublimation ($L_{ws}=2.8 \times 10^6 \text{ J Kg}^{-1}$) depending if the surface is ice or water. q_a and q_s are the air specific humidity and the humidity close to the surface (which is assumed to be at saturation), respectively. q_{su} is given as a function of e_s , the vapour pressure at saturation, and of p_a , the atmospheric pressure:

$$e_s = 611 \times 10^{a(T_a - 273.16)/(T_a - b)} , \quad (70)$$

$$q_{su} = \frac{0.622 e_s}{p_a - 0.378 e_s} , \quad (71)$$

where (a,b) are two coefficients whose values relative to water are (7.5, 35.86) and relative to ice are (9.5, 7.66) (Murray, 1967).

The transfer coefficients c_{sh} and c_{le} over ice-free ocean are computed according to the method of Large and Pond (1981, 1982), with a modification in the computation of z_0 proposed by Oberhuber (1988) to increase the latent heat loss :

$$c_{sh} = 0.0327 \frac{k}{\ln(z/z_0)} \Phi_{sh}(T_a, T_s, q_a, q_s, u_*)$$

$$c_{le} = 0.0346 \frac{k}{\ln(z/z_0)} \Phi_{le}(T_a, T_s, q_a, q_s, u_*) , \quad (72)$$

with z_0 computed for the ocean as :

$$z_0 = c_{char} \frac{u_*^2}{g}, \quad (73)$$

with c_{char} equal to 0.032 (Oberhuber, 1988).

Φ_{sh} and Φ_{le} are two algebraic functions which have been introduced in Eq. (72) to take into account the effects of the stability of the air above the surface. In neutral condition they are equal to 1. In such a case the transfer coefficients are referred as c_{shN} and c_{leN} . The expression of Φ_{sh} and Φ_{le} are given by (e.g., Large and Pond, 1982; Oberhuber, 1988):

$$\begin{aligned} \Phi_{sh}(T_a, T_s, q_a, q_s, u_*) &= \frac{\sqrt{c_M/c_{MN}}}{1 - c_{shN} k^{-1} C_{MN}^{-1/2} \psi_H(Z/L)} \\ \Phi_{le}(T_a, T_s, q_a, q_s, u_*) &= \frac{\sqrt{c_M/c_{MN}}}{1 - c_{leN} k^{-1} C_{MN}^{-1/2} \psi_L(Z/L)} \\ \sqrt{c_M/c_{MN}} &= \left(1 - \sqrt{C_{MN}} k^{-1} \psi_M(Z/L)\right)^{-1} \\ c_{MN} &= \frac{k^2}{\ln^2(Z/z_0)} \\ T_0 &= T_a(1 + 2.2 \times 10^{-3} T_a q_a) \end{aligned} \quad (74)$$

for stable atmospheric conditions

$$\begin{aligned} \psi_M &= \psi_H = \psi_L = -7(Z/L) \\ (Z/L) &= -\frac{70 Z}{T_0 u_*^2 / c_M} \left((T_s - T_a) + 3.2 \times 10^{-3} T_0^2 (q_a - q_s) \right) \end{aligned}$$

for unstable atmospheric conditions

$$\begin{aligned} \psi_M &= 2 \ln[(1 + X)/2] + \ln[(1 + X^2)/2] - 2 \arctan X + \pi/2 \\ \psi_H &= \psi_L = 2 \ln[(1 + X^2)/2] \\ X &= (1 - 16(Z/L))^{1/4} \\ (Z/L) &= -\frac{100 Z}{T_0 u_*^2 / c_M} \left((T_a - T_s) + 2.2 \times 10^{-3} T_0^2 (q_s - q_a) \right) \end{aligned}$$

where Z is the height at which atmospheric data are given.

Over sea ice, it is simply assumed that c_{sh} and c_{le} are constant ($c_{sh} = c_{le} = 1.75 \times 10^{-3}$, Parkinson and Washington, 1979; Maykut, 1982). The theoretical justification of a stability correction seems well established, but the classical formulation is probably not the most appropriate at high latitudes (Overland and Guest, 1991). Furthermore, some tests have been performed with the stability correction showing that it does not modify significantly the results.

The net longwave radiation is parameterized according to Berliand and Berliand (1952) :

$$F_{lw} = \varepsilon_s \sigma T_a^4 \left(0.39 - 0.05 \sqrt{e_a/100}\right) (1 - \chi_{ld}^2) + 4 \varepsilon_s \sigma T_a^3 (T_{su} - T_a), \quad (75)$$

where e_s is the emissivity of the surface and σ is the Stefan-Boltzmann constant. e_a is the vapour pressure of the air. $(1 - \chi c_{ld}^2)$ is a correction factor to account for the effect of the clouds. c_{ld} is the fractional cloud cover ($0 \leq c_{ld} \leq 1$) and χ is a coefficient which increases linearly from the equator (0.5) to the pole (1.0) to roughly take into consideration the various properties of the clouds (Budyko, 1974). Note that the classical emission of the surface $\varepsilon_s \sigma T_s^4$ is already included in Eq. (75).

The solar radiation is computed following the formula of Zillmann (1972). The daily net downward flux is given by :

$$F_s = (1 - \alpha_{su}) \frac{\gamma f_s(c_{ld})}{2\pi} \int_{t_1}^{t_2} \frac{S_0 \cos^2 \mu}{1.085 \cos \mu + (2.7 + \cos \mu) e_a \times 10^{-3} + 0.1} dt , \quad (76)$$

where t_1, t_2 are the time of sunrise and sunset, respectively, S_0 is the solar constant (=1370 W/m²). γ is a correction factor introduced by Oberhuber ($\gamma=0.9$) during is tuning of the various parameterizations. α_{su} is the albedo, and $f_s(c_{ld})$ is a cloud correction. $\cos \mu$ is computed by :

$$\begin{aligned} \cos \mu &= \sin \varphi \sin \delta + \cos \varphi \cos \delta \cos HA , \\ \delta &= 23.44^\circ \cos \left[\left(172 - \text{day of the year} \right) \pi / 180 \right] , \\ HA &= 12 \text{ hours} - \text{Solar time} , \end{aligned} \quad (77)$$

where φ is the latitude.

The cloud correction is taken from Reed (1977) :

$$f_s(c_{ld}) = 1 - 0.62 c_{ld} + 0.0019 \mu_{noon} , \quad (78)$$

where μ_{noon} is the noon solar altitude. It is further imposed that $f_s(c_{ld})$ is lower than 1.

While Oberhuber (1988) assumes that the albedo of seawater is constant ($\alpha_{su}=0.06$), a simplified version of the parameterization of Payne (1972) is used here. α_{su} is equal to 0.06 for totally overcast conditions and for clear sky conditions:

$$\alpha_{su} = \frac{0.05}{1.1(\cos \mu)^{1.4} + 0.15} . \quad (79)$$

A linear interpolation between these two extreme values in function of c_{ld} is then applied.

For highly reflective surfaces such as sea ice, it may be necessary to take into account multiple reflections between the clouds and the surface. Therefore, for ice and snow, the parameterization of Shine (1984) which is specifically adapted for computing the shortwave flux on high albedo surfaces is used instead of Eq. (76):

For cloudy conditions :

$$F_s = \frac{1}{2\pi} \int_{t_1}^{t_2} \frac{(53.5 + 1274.5 \cos \mu) (\cos \mu)^{0.5} (1 - 0.996 \alpha_{su})}{1 + 0.0139 (1 - 0.9435 \alpha_{su}) \tau_c} dt . \quad (80)$$

For clear sky :

$$F_s = \frac{1}{2\pi} \int_{t_1}^{t_2} \frac{1368 \cos^2 \mu (1 - \alpha_{su})}{1.2 \cos \mu + (1.0 + \cos \mu) e_a \times 10^{-3} + 0.0455} dt . \quad (81)$$

A linear interpolation is applied to obtain a value for an intermediate cloud cover. τ_c is the optical thickness of the clouds which depends on the latitude as in Chou and Curran (1981).

The albedo for snow and ice (α_{su}) is a function of the surface characteristics (snow or not, melting or not, ice and snow thicknesses) as proposed by Shine and Henderson-Sellers (1985). Furthermore, as suggested by Grenfell and Perovich (1984), the albedo is increased by 0.06 for albedos larger than 0.28 under overcast conditions to take into account the selective absorption of shortwave radiation by clouds.

In addition to (76), (80), and (81) a correction has been introduced to take into account the variation of the distance between the sun and the earth during the year (Oberhuber, 1988):

$$F_{sc} = F_s \left(1 + 0.0013 \sin \left(\text{day of the year} \frac{2\pi}{365} \right) + 0.0342 \sin \left(\text{day of the year} \frac{2\pi}{365} \right) \right) \quad (82)$$

The latent heat, sensible heat, and infrared heat fluxes can be safely considered as surface fluxes, all the exchanges taking place in the top centimetre or so. However, that is not at all true for the solar radiation, a significant amount of heat being absorbed in the ocean at depth. To take this effect into account, it is assumed that the extinction of solar radiation follows the parameterization of Paulson and Simpson (1977) :

$$\frac{F_s(z)}{F_s(0)} = R e^{-\zeta_1 z} + (1 - R) e^{-\zeta_2 z} , \quad (83)$$

where $F_s(z)$ is the solar irradiance at depth z . R , ζ_1 , and ζ_2 are empirical coefficients (Paulson and Simpson, 1977) which depend on the water type (Jerlov, 1976). The geographical distribution of the water types is taken from the work of Simonot and Letreut (1986). The same procedure is applied for the solar flux which is coming to the ocean through the ice.

Table 4. Atmospheric data used in the computation of the surface forcing

Variable	Climatology
Air temperature (T_a)	Crutcher and Meserve, 1970; Taljaard et al., 1969 or NCEP/NCAR reanalyses (Kalnay et al, 1996)
Atmospheric pressure (p_a)	Crutcher and Meserve, 1970; Taljaard et al., 1969
Air relative humidity (f_a)	Trenberth et al., 1989 (based on COADS data set)
Cloud cover (cl_d)	Berliand and Strokina, 1980
Wind speed (V_a)	Trenberth et al., 1989; Hellerman and Rosenstein, 1983 or NCEP/NCAR reanalyses (Kalnay et al, 1996)
Wind stress (τ_s)	Trenberth et al., 1989; Hellerman and Rosenstein, 1983 or NCEP/NCAR reanalyses (Kalnay et al, 1996)
Precipitation	Xie and Arkin, 1996

In the previous versions, the atmospheric data needed in the bulk formulae were always taken from monthly mean climatologies (Table 4). The fluxes generated by these monthly mean data may be different than the mean flux obtained from instantaneous values, because of the non-linearities of the formulas. However, Esbensen and Reynolds (1981), by comparing the results given by the two methods indicate that the difference are of the order of a few percent. This seems to be confirmed by the more recent work of Simmons and Dix (1989) which is based on the outputs of an atmospheric model. But, these conclusions are probably not valid everywhere. For example, Gulev (1994) or Staneva et al.(1995) have found errors greater than 40% when monthly mean values are used to compute the flux. The problems can also be important for the transfer of momentum and more critically for the turbulent kinetic energy . The monthly mean data are easier to handle than daily variables. Furthermore, climatological data are generally given in monthly means. Nevertheless, because of these problems associated with monthly mean values, a modification has been introduced in the new version to allow the use of use daily values for the air temperature, wind speed and wind stress.

5.2. Surface flux of freshwater

The surface flux of freshwater results from the difference between precipitation and evaporation. The latter can be simply computed from the latent heat flux (Eq. 69):

$$E_{vap} = \frac{F_{le}}{L_w} , \quad (84)$$

The precipitation rates are taken from the merged analysis of Xie and Arkin (1996), which is an objective combination of gauge observation, satellite estimates, and numerical predictions. It gives monthly mean values based on data from years 1979 to 1995.

A part of the precipitation is falling as snow. This amount is determined as in Ledley (1985), who assumes that the percentage of snow is equal to 1 if the air temperature is lower than -20°C , decreases linearly between -20° and $+8^{\circ}\text{C}$ to reach 0 at $+8^{\circ}\text{C}$ and above. The snow falling on the ice can accumulate, but it melts immediately in leads and open water. The latent heat necessary for this snow melt is taken from the ocean. The rain falling on the ice percolates through the ice and reaches the ocean.

The river runoff is also considered as a purely surface forcing as the rivers generally discharge their water into the ocean at a depth of the order of the model surface level. The monthly mean data base of the GRDC (Global Runoff Data Centre, Grabs et al., 1996) is used for the major rivers of the World. However, this climatology takes into account only a small part of the World's rivers, the total freshwater flux to the ocean being about one half of the value generally admitted (Grabs et al., 1996). To cope with this problem, another data set has been added. In every group of three grid points close to the coast, the total annual mean discharge is not allowed to be lower than the value deduced from the annual mean climatology of Baumgartner and Reichel (1975). If this occurs, a complementary water discharge (constant throughout the year) is introduced. This technique permits a total amount of freshwater transport to the ocean which has the same magnitude as in Baumgartner and Reichel (1975) (difference of a few percent), while keeping the seasonal cycle for the major rivers.

Two supplementary freshwater fluxes due to glacial melting have been introduced. Iceberg melting is assumed to occur uniformly southward of 55°S (iceberg

melting is neglected in the Northern Hemisphere). The estimation of total iceberg discharge of Jacobs et al. (1992) gives a value of about 10 cm/year. The direct melting of the ice shelves at the interface with seawater (along vertical walls and below the floating part of the ice shelves) is also taken into account. The meltwater volume estimated by Jacobs et al. (1992) has been distributed over the whole Antarctic continental shelf, inducing a mean flux of 23 cm/year. It is considered as a surface flux, because more precise information are not easily available.

The error on the freshwater can be quite significant: the latent heat flux computed by the bulk method has probably an uncertainty of 25% (Weare, 1991); precipitation over the ocean is difficult to estimate, because the classical gauge method is not well adapted and because of the spatial and temporal variability of precipitation (e.g., Dorman and Bourke, 1979; Xie and Atkin, 1996). Furthermore, there is no direct feedback between the freshwater flux and the characteristics of the ocean surface, as it the case for temperature. As a consequence, the sea-surface salinity can strongly drift, even for a small error in the freshwater flux. To avoid this salinity drift, a correction has been introduced by means of a surface salt flux :

$$F_S = \frac{\Delta z_{su}}{\tau_r} (S_{obs} - S_{su}), \quad (85)$$

where Δz_{su} is the thickness of the surface grid box and τ_r is a characteristic time scale for the restoring. S_{obs} is the annual mean salinity of Levitus (1982) and S_{su} the model surface salinity. A relatively long time scale of 2 month is applied here in order to do not mask the effects of precipitation, evaporation, runoff, and mass exchange with the ice. This gives a value¹⁴ of $\Delta z_{su} / \tau_r = 1.9 \times 10^{-6}$ m/s. This can be compared to other models which used only surface restoring (no freshwater flux) and then need a stronger value. For example, Reason and Power (1994) have $\Delta z_{su} / \tau_r = 1.4 \times 10^{-5}$ m/s ($\tau_r = 20$ days, $\Delta z_{su} = 25$ m) and Campin (1997) uses $\Delta z_{su} / \tau_r = 2.9 \times 10^{-5}$ m/s ($\tau_r = 8$ days, $\Delta z_{su} = 20$ m).

In the model there is two ways to represent the freshwater flux at the ocean surface: it is modelled as an equivalent salt flux or as a realistic freshwater flux. In the first approach only the dilution effect of the freshwater flux is taken into account. Its is thus equivalent to a negative salt flux (e.g., Bryan, 1969; Bryan and Lewis, 1979; Campin, 1997)¹⁵ :

$$F_{Seq} = -S_{oce} (Precip - E_{vap} + Runoff), \quad (86)$$

where S_{oce} is a characteristic salinity for the ocean surface ($S_{oce} = 34.7$ psu). A constant salinity has been chosen rather than the more logical local salinity so that a globally balanced freshwater flux is associated with a globally balanced salt flux.

An other alternative, proposed by the model, is to introduce the freshwater flux in a more realistic way as suggested by Huang (1993). This approach is used in the standard version of the model. A vertical velocity W^+ , positive upward, is imposed at the sea surface. $W^+ = -Precip + Evapo - Runoff$ is the opposite of the net freshwater flux. It is

¹⁴ This corresponds to an equivalent freshwater flux of 0.18 m/year if the difference of salinity between model and observation is equal to 0.1 psu.

¹⁵ In partially ice-covered grid points, this forcing must be multiplied by (1-A), the percentage of lead, the effect of the ice being described by Eq. (II.66).

positive/negative in regions of net evaporation/precipitation. This vertical velocity has an impact on the continuity equation, on the sea-surface elevation, and also on the three-dimensionnal velocity field. This alternative induces a clearer representation of the oceanic freshwater transport than the virtual salt flux approach.

Keeping the restoring term as a salt flux at the sea surface, whereas W^+ is a freshwater flux, will introduce a drift both in the oceanic salt content and in the total volume of the ocean. Assuming a positive/negative net freshwater flux towards the ocean, the additional restoring term will tend to maintain an almost constant sea-surface salinity and act as a source/sink of salt for the ocean. In order to overcome this problem, it is necessary to convert the salt flux due to the restoring term into a freshwater flux positive downward

$$F_f = -\frac{\Delta z_{su}}{S_{su} \cdot \tau_r} (S_{obs} - S_{su}). \quad (87)$$

This flux is therefore included in W^+ .

5.3. Surface flux of momentum and surface boundary condition for the turbulent kinetic energy.

The surface wind stress is based on the atlas of Trenberth et al. (1989) who computed the stress from twice-daily ECMWF winds, using the drag coefficients of Large and Pond (1981) slightly modified in case of low wind speeds. As argued by Trenberth et al. (1989), the results do not seem to be reliable in tropical regions. Therefore, between 15°S and 15°N, the classical climatology of Hellerman and Rosenstein (1983) is used to force the model, a transition region 5° wide being applied between the two data sets. Furthermore, Trenberth et al.'s (1989) surface wind stresses are too strong. This is mainly due to the fact that they assume that the wind at 1000 hPa can be considered as surface wind (because during a large part of the period studied, the surface observations were assimilated at this height). But, this hypothesis does not appear to be valid (Mestas-Nuñez et al., 1994). As a consequence, the wind speed has been reduced everywhere by 10% (thus 19% for the wind stress), as done for example in the OPYC model when using Trenberth et al.'s (1989) wind stresses (D. Holland, 1994, personal communication). This value is still lower than the one proposed by Mestas-Nuñez et al. (1994), deduced from a comparison of the stresses measured from the scatterometer SASS (Seasat A Satellite Scatterometer) to Trenberth et al.'s (1989) results (14% of reduction for wind speed, 46% for the wind stress).

The following boundary condition for q^2 (twice the turbulent kinetic energy) is applied at the surface ($z=0$) of the water column (Mellor and Yamada, 1982) :

$$q^2 = B_1^{2/3} u_*^2. \quad (88)$$

In order to limit the underestimation of the wind transfer to the ocean caused by the use of a monthly mean forcing, the friction velocities are directly taken from the climatology computed with daily data (Trenberth et al., 1989). Below the ice, it is assumed that the square of the friction velocity is reduced by a factor $|\tau_s|/|\tau_{iw}|$ to take into account the effect of ice dynamics.

Furthermore, at the first grid interface below the surface, it is imposed that

$$q^2 \geq B_1^{2/3} u_*^2, \quad (89)$$

$$l \geq kz, \quad (90)$$

where z is the depth of the first interface and l is the mixing length. This approach is somewhat similar to the one proposed by Lynch et al. (1995) for the logarithmic boundary layer and allows a better mixing between the first and second levels of the model.

5.4. Lateral and bottom boundary conditions

It is assumed that no exchange of heat or salt occurs between the ocean and the land (bottom and coast). On the lateral boundary, the no-slip condition is used (velocity equal to zero). At the bottom, a quadratic stress is applied :

$$\tau_{bot} = \rho_0 c_{db} |\mathbf{u}_{bot}| \mathbf{u}_{bot} \quad (91)$$

where \mathbf{u}_{bot} is the velocity at the bottom of the ocean and c_{db} a drag coefficient ($c_{db}=1.5 \times 10^{-3}$).

For the bottom boundary condition on turbulent kinetic energy, an equation similar to Eq. (88) is used.

6. The evolution of CFCs

The simulation of uptake and redistribution of Chloro-Fluoro-Carbons (CFCs) in a large-scale ocean model has proven to be a helpful tool for model validation (England et al., 1994; England, 1995; England and Hirst, 1997). By comparing the model results with the observations, it is possible to obtain interesting information on the model behaviour, complementary to what can be deduced from the analysis of classical variables such as temperature and salinity. In particular, the CFCs are very useful to study the ventilation of the ocean on annual to decadal time scales, since their release into the atmosphere (because of human activities) has begun in the 1930's.

The CFCs have another advantage for modelling studies compared to other tracers (anthropogenic or not): they are very stable and not affected by biological processes. As a consequence, their evolution in the ocean interior is only due to physical processes and can be represented by a "simple" advection-diffusion equation (keeping the same notation and hypothesis than in sub-section 2.1)

$$\frac{\partial CFC}{\partial t} + \mathbf{u} \cdot \nabla_h CFC + w \frac{\partial CFC}{\partial z} = A_s \nabla_h^2 CFC + \frac{\partial}{\partial z} K_s \frac{\partial CFC}{\partial z}, \quad (92)$$

where CFC is the concentration of dissolved CFC (CFC-11 or CFC-12).

The only source of CFC is the surface boundary condition. In the present study, the comprehensive parameterization of England et al.(1994) (their parameterisation 4) is used as in England (1995) or in England and Hirst (1997). The flux across the air-sea interface is given by (Liss and Merlivat, 1986; Wanninkof, 1992) :

$$F_{CFC} = k_c (\alpha_c C_{atm} - CFC_{su})(1 - A), \quad (93)$$

where k_c is the gas transfer speed for CFC, α_c is the solubility coefficient, C_{atm} is the atmospheric dry air mole fraction, and CFC_{su} is the gas concentration in surface waters. $\alpha_c C_{atm}$ is the water concentration in equilibrium with the atmospheric value C_{atm} . The factor $(1-A)$ is introduced to take into account the strong reduction of air-ocean transfer in presence of ice.

The solubility of CFC-11 and CFC-12 is a function of salinity and temperature as given by Warner and Weiss (1985):

$$\ln \alpha_c = a_1 + a_2 \left(\frac{100}{T} \right) + a_3 \ln \left(\frac{T}{100} \right) + a_4 \left(\frac{T}{100} \right)^2 + S \left[b_1 + b_2 \left(\frac{T}{100} \right) + b_3 \left(\frac{T}{100} \right)^2 \right] \quad (94)$$

with $(a_1, a_2, a_3, a_4, b_1, b_2, b_3) = (-232.0411, 322.5546, 120.4956, -1.39165, -0.146531, 0.093621, -0.0160693)$ for CFC-11 and $(a_1, a_2, a_3, a_4, b_1, b_2, b_3) = (-220.2120, 301.8695, 114.8533, -1.39165, -0.147718, 0.093175, -0.0157340)$ for CFC-12

The gas-transfer speed is a function of the wind speed and Schmidt number (Sc) as proposed in the formulation of Wanninkof (1992), which is adapted for climatological wind data such the ones used here:

$$k_c = \frac{k_0 V_a^2}{\sqrt{Sc}}, \quad (95)$$

where k_0 is a constant (7.964). The Schmidt number for the corresponding gas is given by (Wanninkof, 1992) :

$$Sc = A - B (T - 273.15) + C (T - 273.15)^2 - D (T - 273.15)^3, \quad (96)$$

with $(A, B, C, D) = (3713.2, 243.30, 7.5879, 0.095215)$ for CFC-11 and $(A, B, C, D) = (4039.8, 264.70, 8.2552, 0.10359)$ for CFC-12.

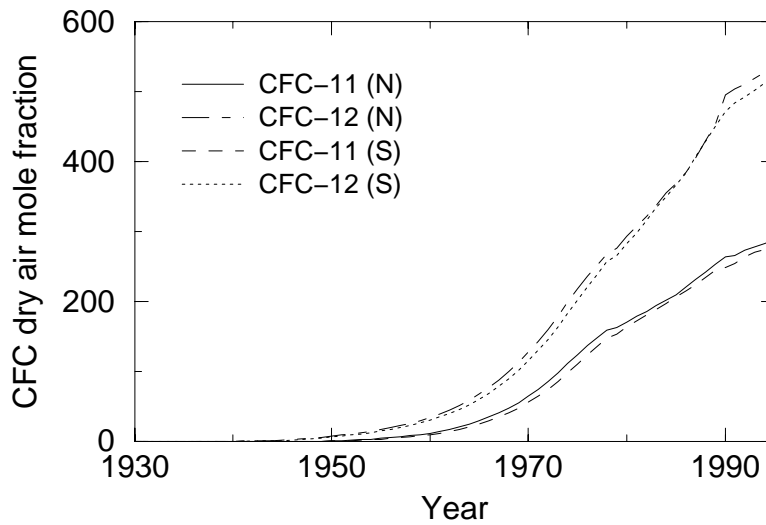


Fig. 6 Time evolution of the atmospheric dry air mole fraction of CFC-11 and CFC-12 (in ppt) for both hemispheres (N and S).

The dry air mole fraction of CFCs is supposed to be a simple function of the hemisphere and the time (England et al. 1994). Fig. 6 displays the estimated values, based on the work of Warner and Weiss (1992), Doney and Bullister (1992), and Elkins et al. (1993). The CFC concentration is a little lower in the Southern Hemisphere because nearly all the production and release of CFC occurs in the Northern Hemisphere. However, the rapid mixing in the lower troposphere induces a relatively fast homogenisation of the gas and a lag of only a few years in Southern Hemisphere concentration.

References

- Bauer J. and S. Martin (1983). *A model of grease ice growth in small leads*. J. Geophys. Res. **88**(C5), 2917-2925
- Baumgartner A. and E. Reichel (1975). *The world water balance*. Elsevier, Amsterdam
- Beckers J.M. and E. Deleersnijder (1993). *Stability of the FBTCS scheme applied to the propagation of shallow-water inertia-gravity waves on various space grids*. J. Comput. Phys **108**, 95-104
- Beckmann A. and R. Döscher (1997). *A method for improved representation of dense water spreading over topography in geopotential-coordinate models*. J. Phys. Oceanogr. **27**, 581-591
- Berliand M.E. and T.G. Berliand (1952). *Determining the net long-wave radiation of the earth with consideration of the effect of cloudiness* (in Russian). Isv. Akad. Nauk. SSSR Ser. Geophys, No 1.
- Berliand M.E. and T.G. Strokina (1980). *Global distribution of the total amount of clouds* (in Russian). Hydrometeorological Publishing House, Leningrad, Russia, 71 pp.
- Blanc T.V. (1985). *Variation of bulk-derived surface flux, stability, and roughness results due to the use of different transfer coefficient schemes*. J. Phys. Oceanogr. **15**, 650-669
- Blanc T.V. (1987). *Accuracy of bulk-method-determined flux, stability, and sea surface roughness*. J. Geophys. Res. **92**(C4), 3867-3876
- Blanke B. and P. Delecluse (1993). *Variability of the tropical Atlantic Ocean simulated by a general circulation model with two different mixed-layer physics*. J. Phys. Oceanogr. **23**, 1363-1388
- Bryan K. (1969). *A numerical method for the study of the circulation of the world ocean*. J. Comput. Phys. **4**, 347-376
- Bryan K. and L.J. Lewis (1979). *A water mass model of the world ocean*. J. Geophys. Res. **84** (C5), 2503-2517
- Bryan K. (1984). *Accelerating the convergence to equilibrium of ocean-climate models*. J. Phys. Oceanogr. **14**, 666-673.
- Budyko M.I. (1974). *Climate and life*. Academic Press, New York, 508pp.
- Campin J.M. (1997). *Modélisation tridimensionnelle de la circulation générale océanique lors du dernier maximum glaciaire*. PhD Thesis, Université Catholique de Louvain, Louvain-la-Neuve, Belgium. 342pp
- Campin J.M. and H. Goosse (1999). *A parameterization of density driven downsloping flow for coarse resolution model in z-coordinate*. Tellus **51A**, 412-430
- Chapman D.C. and G. Gawarkiewicz (1995). *Offshore transport of dense shelf water in the presence of a submarine canyon*. J. Geophys. Res. **100**(C7), 13373-13387
- Chou S.-H. and R.J. Curran (1981). *The effects of surface evaporation parameterizations on climate sensitivity to solar constant variations*. J. Atmos. Sci. **38**, 931-938

- Cox G.F.N. and W.F. Weeks (1974). *Salinity variations in sea ice*. J. Glaciol. **13**(67), 109-120
- Cox G.F.N. and W.F. Weeks (1988). *Numerical simulations of the profile properties of undeformed first-year sea ice during the growth season*. J. Geophys. Res. **93** 12449-12460
- Crutcher H.L. and J.M. Meserve (1970). *Selected level heights, temperatures and dew points for the Northern Hemisphere*. Naval Weather Service, NAVAIR 50-1C-52 Revised, Washington D.C.
- Cushman-Roisin B. (1994). *Introduction to geophysical fluid dynamics*. Prentice Hall, Englewood Cliffs, New Jersey, 320 pp.
- Da Silva A.M., C.C. Young and S. Levitus (1994). *Atlas of surface marine data 1994. Vol.1: Algorithms and procedures*. US Dept. of commerce. NOAA Atlas NESIDS 6, Washington D.C., USA, 83 pp.
- Deleersnijder E. (1992). *Modélisation hydrodynamique tridimensionnelle de la circulation générale estivale de la région du Détroit de Bering*. PhD Thesis, Université Catholique de Louvain, Louvain-la-Neuve, Belgium. 189pp
- Deleersnijder E., J.P. van Ypersele and J.M. Campin (1993) *An orthogonal curvilinear coordinate system for a World Ocean model*. Ocean Modell. **100**, 7-10 (+figures)
- Deleersnijder E. and P. Luyten (1994). *On the practical advantages of the quasi-equilibrium version of the Mellor and Yamada level 2.5 turbulence closure applied to marine modelling*. Appl. Math. Modelling **18**, 281-287
- Deleersnijder E. and J.M. Campin (1995). *On the computation of the barotropic mode of a free-surface world ocean model*. Ann. Geophys. **13**, 675-688
- Dobson F.W. and S.D. Smith (1988). *Bulk models of solar radiation at sea*. Quart. J. R. Met. Soc. **114**, 165-182.
- Doney S.C. and J.L. Bullister (1992). *A chlorofluorocarbon section in the eastern North Atlantic*. Deep Sea Res. **39**(11/12), 1857-1883.
- Dorman C.E. and R.H. Bourke (1979). *Precipitation over the Pacific Ocean, 30°S to 60°N*. Month. Weath. Rev. **107**, 896-910.
- Drijfhout S., C. Heinze, M. Latif and E. Maier-Reimer (1996). *Mean circulation and internal variability in an ocean primitive equation model*. J. Phys. Oceanogr. **26**, 559-580
- Ebert E.E. and J.A. Curry (1993). *An intermediate one-dimensional thermodynamic sea ice model for investigating ice-atmosphere interactions*. J. Geophys. Res. **98**(C6), 10085-10109
- Elkins J.W., T.M. Thompson, T.H. Swanson, J.H. Butler, B.D. Hall, S.O. Cummings, D.A. Fisher and A.G. Raffo. *Decrease in the growth rates of atmospheric chlorofluorocarbons 11 and 12*. Nature **364**, 780-783
- England M.H. (1993) *Representing the global-scale water masses in ocean general circulation models*. J. Phys. Oceanogr. **23**, 1523-1552
- England M.H., V. Garçon and J.-F. Minster (1994). *Chlorofluorocarbon uptake in a World Ocean model 1. Sensitivity to the surface gas forcing*. J. Geophys. Res. **99**(C12), 25215-25233

- England M. H. (1995). *Using chlorofluorocarbons to assess ocean climate models*. Geophys. Res. Let. **22**(22) 3051-3054
- England M. H. and A.C. Hirst (1997). *Chlorofluorocarbon uptake in a World Ocean model 2. Sensitivity to surface thermohaline forcing and subsurface mixing parameterisations*. J. Geophys. Res. **102**(C7), 15709-15731
- Esbensen S.K. and R.W. Reynolds (1981). *Estimating monthly averaged air-sea transfers of heat and momentum using the bulk aerodynamic method*. J. Phys. Oceanogr. **11**, 457-465
- ETOPO 5 (1986). *Global 5' times 5' Depth and Elevation*. Available from National Geophysical Data Center, NOAA, US Dept of Commerce, Code E/GC3, Boulder, CO 80303
- Fichefet T. and P. Gaspar (1988). *A model study of upper ocean-sea ice interactions*. J. Phys. Oceanogr. **18**, 181-195
- Fichefet T. and M. A. Morales Maqueda (1997). *Sensitivity of a global sea ice model to the treatment of ice thermodynamics and dynamics*. J. Geophys. Res. **102**(C6), 12609-12646
- Fichefet T. and M. A. Morales Maqueda (1999). *Modelling the influence of snow accumulation and snow-ice formation on the seasonal cycle of the Antarctic sea-ice cover*. Clim Dyn. **15**(4), 251-268
- Fichefet T., and H. Goosse, 1999. *A numerical investigation of the spring Ross sea polynya*. Geophys. Res. Let. **26**(8), 1015-1018
- Fichefet T., B. Tartinville and H. Goosse, 2000. *Sensitivity of the Antarctic sea-ice to the thermal conductivity of snow*. Geophys. Res. Let. **27**(3), 401-404
- Foldvik A., T. Gammelsrød and T. Tørresen (1985). *Circulation and water masses on the southern Weddell Sea shelf*. In, *Oceanology of the Antarctic Continental Shelf*. Antarctic Research Series **43**, Amer. Geophys. Union, 5-20
- Foster T.D. and E.C. Carmack (1976). *Frontal zone mixing and Antarctic Bottom Water formation in the southern Weddell Sea*. Deep Sea Res. **23**, 301-317.
- Foster T.D., A. Foldvik and J.H. Middleton (1987). *Mixing and bottom water formation in the shelf break region of the southern Weddell Sea*. Deep Sea Res. **34**(11), 1771-1794
- Fung I.Y., D.E. Harrison and A.A. Lacis (1984). *On the variability of the net longwave radiation at the ocean surface*. Rev. Geophys. Space. Phys. **22**(2) 177-193.
- Gadd A.J. (1978). *A split-explicit integration scheme for numerical weather prediction*. Q. J. R. Meteorol. Soc. **104**, 569-582.
- Galperin B., L.H. Kantha, S. Hassid and A. Rosati (1988). *A quasi-equilibrium turbulent energy model for geophysical flows*. J. Atmos. Sciences **45**, 55-62
- Gaspar P., Y. Grégoris and J.M. Lefevre (1990). *A simple eddy kinetic energy model for simulations of the oceanic vertical mixing : tests at station papa and long-term upper ocean study site*. J. Geophys. Res. **95**(C9), 16179-16193
- Gawarkiewicz G. and D.C. Chapman (1995). *A numerical study of dense water formation and transport on a shallow, sloping continental shelf*. J. Geophys. Res. **100**(C3), 4489-4507

- Gent P.R. and J.C. McWilliams (1990). *Isopycnal mixing in ocean general circulation models*. J. Phys. Oceanogr. **20**, 150-155
- Gill A. E. (1973). *Circulation and bottom water production in the Weddell Sea*. Deep-Sea Res. **20**, 111-140
- Gill A. E. (1982). *Atmosphere-Ocean Dynamics*. International Geophysics Series, 30 Academic Press, San Diego, 662 pp.
- Goosse H. (1995). *Development of a global coupled sea-ice ocean model*. Progress Report 1995/5. Institut d'Astronomie et de Géophysique G. Lemaître, Louvain-la-Neuve, Belgium, 25pp.
- Goosse H., T. Fichefet, M.A. Morales Maqueda, J.-M. Campin and E. Deleersnijder (1996). *On the dynamical coupling of large-scale ocean and sea-ice models*. Bul. Soc. Roy. Sc. Liège **65**, 87-90
- Goosse H., J.-M. Campin, T. Fichefet and E. Deleersnijder (1997a). *Sensitivity of a global ice-ocean model to the Bering Strait throughflow*. Clim. Dyn. **13**, 349-358
- Goosse H., J.M. Campin, T. Fichefet and E. Deleersnijder (1997b). *The impact of sea-ice formation on the properties of Antarctic Bottom Water*. Ann. Glaciol. **25**, (in press)
- Goosse H., T. Fichefet and J.-M. Campin (1997c). *The effects of the water flow through the Canadian Archipelago in a global ice-ocean model*. Geophys. Res. Lett., **24**(12), 1507-1510
- Goosse, H., E. Deleersnijder, T. Fichefet and M.H. England (1998). *Sensitivity of a global coupled ocean-sea ice model to the parameterization of vertical mixing*. J. Geophys. Res. **104**(C6), 13681-13695
- Goosse H., and T. Fichefet, 1999. Importance of ice-ocean interactions for the global ocean circulation: a model study. J. Geophys. Res. **104**(C10) 23337-23355.
- Gordon A. L. (1991) *Two stable modes of Southern Ocean winter stratification*. In, *Deep convection and deep water formation in the oceans*, Chu and Giscard (editors). Elsevier Oceanography series 57, Elsevier, Amsterdam, Netherlands, 17-35
- Gow A.J. and W.B. Tucker (1990). *Sea ice in polar regions*. In, *Polar Oceanography, Part A, Physical Science*, W.O. Smith (Editor), Academic press, San Diego, USA, pp. 47-122.
- Grabs W., T. De Couet and J. Pauler (1996). *Freshwater fluxes from continents into the world oceans based on data of the global runoff data base*. Global Runoff Data Centre Report 10, Federal Institute of Hydrology, Koblenz, Germany.
- Grenfell T.C. and G.A. Maykut (1977). *The optical properties of ice and snow in the Arctic Basin*. J. Glaciol. **18**, 445-463.
- Gulev S.K. (1994). *Influence of space-time averaging on the ocean-atmosphere exchanges estimates in the North Atlantic midlatitudes*. J. Phys. Oceanogr. **24**, 1236-1255.
- Häkkinen S. and G.L. Mellor (1992). *Modeling the seasonal variability of a coupled Arctic ice-ocean system*. J. Geophys. Res. **97**(C12), 20285-20304.
- Hellerman S. and M. Rosenstein (1983). *Normal monthly wind stress over the World Ocean with error estimates*. J. Phys. Oceanogr. **13**, 1093-1104.

- Hopkins M.A., W.D. Hibler and G.M. Flato (1991). *On the numerical simulation of the sea ice ridging process*. J. Geophys. Res. **96**(C3), 4809-4820
- James I.D. (1986). *A front-resolving sigma coordinate sea model with a simple hybrid advection scheme*. Appl. Math. Modelling **10**, 87-92
- Jiang L. and R.W. Garwood (1995). *A numerical study of three-dimensional dense bottom plumes on a Southern Ocean continental slope*. J. Geophys. Res. **100**(C9), 18471-18488
- Jiang L. and R.W. Garwood (1996). *Three-dimensional simulations of overflows on continental slopes*. J. Phys. Oceanogr. **26**, 1214-1233
- Harvey L.D.D. (1996). *Polar boundary layer plumes and bottom water formation: a missing element in ocean general circulation models*. J. Geophys. Res. **101** (C9), 20799-20808.
- Hibler W.D. (1979). *A dynamic thermodynamic sea ice model*. J. Phys. Oceanogr. **9**, 815-846
- Hirst A.C. and W. Cai (1994). *Sensitivity of a world ocean GCM to changes in subsurface mixing parameterization*. J. Phys. Oceanogr. **24**, 1256-1279
- Huang RX (1993). *Real Freshwater Flux as a Natural Boundary Condition for the Salinity Balance and Thermohaline Circulation Forced by Evaporation and Precipitation*. J. Phys. Oceanogr. **23**, 2428-2446
- Hunkins K. (1975). *The oceanic boundary layer and stress beneath a drifting ice floe*. J. Geophys. Res. **80** (24) 3425-3433
- Jacobs S.S., H.H. Helmer, C.S.M. Doake, A. Jenkins and R.M. Frolich (1992). *Melting of ice shelves and the mass balance of Antarctica*. J. Glaciol. **38**(130), 375-387
- Jerlov N.G. (1976). *Marine optics*. Elsevier Oceanogr. Ser., **14**, Elsevier, Amsterdam, Netherlands, 231 pp.
- Kalnay, E. and XXI others (1996). *The NCEP/NCAR 40-year reanalysis project*. Bull. Amer. Meteor. Soc. **77**, 437-471.
- Kantha L.H. and C.A. Clayson (1994). *An improved mixed layer model for geophysical applications*. J. Geophys. Res. **99**(C12), 25235-25266
- Katsaros K.B. (1990). *Parameterization schemes and models for estimating the surface radiation budget*. In, *Surface waves and fluxes, Volume II*, G.L. Geernaert and W.J. Plant (editors). Kluwer Academic Publishers, Netherlands, 339-368.
- Killworth P.D. (1983). *Deep convection in the world ocean*. Rev. Geophys. Spac. Phys. **21**(1), 1-26
- Killworth P.D., J.M. Smith and A.E. Gill (1984). *Speeding up ocean circulation models*. Ocean Modell. **56**, 1-4.
- Killworth P.D., D. Stainforth, D.J. Webb and S.M. Paterson (1991). *The development of a free-surface Bryan-Cox-Semtner model*. J. Phys. Oceanogr. **21**, 1333-1348
- Klinger B.A., J. Marshall and U. Send (1996). *Representation of convective plumes by vertical adjustment*. J. Geophys. Res. **101**(C8), 18175-18182
- Large W.G. and S. Pond (1981). *Open ocean momentum flux measurements in moderate to strong winds*. J. Phys. Oceanogr. **11**, 324-336.

- Large W.G. and S. Pond (1982). *Sensible and latent heat flux measurements over the ocean*. J. Phys. Oceanogr. **12**, 464-482.
- Large W.G., J.C. McWilliams and S.C. Doney (1994). *Oceanic vertical mixing: a review and a model with a nonlocal boundary layer parameterization*. Rev. Geophys. **32**, 363-403
- Liss P.S. and L. Merlivat (1986). *Air-sea exchange rates: introduction and synthesis*. In, *The role of air-sea exchange in geochemical cycling*, P.Buat-Menard (Editor). Reidel, Dordrecht, Netherlands, 113-127.
- Ledley T.S. (1985). *Sensitivity of a thermodynamic sea ice model with leads to time step size*. J. Geophys. Res. **90**(D1), 2251-2260
- Levitus S. (1982) *Climatological atlas of the World Ocean*. Nat Ocean Atmos Adm Prof Pap 13, US Gov Printing Office, Washington DC
- Lynch D.R., J.T.C. Ip, C.E. Naimie and F.E. Werner (1995). *Convergence studies of tidally-rectified circulation on Georges Bank*. In, *Quantitative skill assessment for coastal ocean models*, eds. D.R. Lynch and A.M. Davies, American Geophysical Union, 47, Washington D.C., 153-174
- Maier-Reimer E., U. Mikolajewicz and K. Hasselmann (1993). *Mean circulation of the Hamburg LSG OGCM and its sensitivity to the thermohaline surface forcing*. J. Phys. Oceanogr. **23**, 731-757
- Marotzke J. (1991). *Influence of convective adjustment on the stability of the thermohaline circulation*. J. Phys. Oceanogr. **21**, 903-907
- Mathieu P.-P., J.-M. Campin and E. Deleersnijder (1996). *Introduction of isopycnal diffusion in the UCL's world ocean model: Preliminary results*. Bul. Soc. Roy. Sc. Liège **65**, 135-138
- Maykut G.A. (1982). *Large-scale heat exchange and ice production in the Central Arctic*. J. Geophys. Res. **87**(C10), 7971-7984
- Maykut G.A. and N. Untersteiner (1971). *Some results from a time-dependent thermodynamic model of sea ice*. J. Geophys. Res. **76**(6), 1550-1575
- McPhee M.G. (1986) *The upper ocean* In, *The geophysics of sea ice*, N. Untersteiner (editor). NATO ASI Series Vol 146. Plenum Press, New-York, 339-394
- McPhee M G., G.A. Maykut and J.H. Morison (1987). *Dynamics and thermodynamics of the ice/upper ocean system in the marginal ice zone of the Greeland Sea*. J. Geophys. Res. **92** (C7), 7017-7031
- McPhee M G (1992) *Turbulent heat flux in the upper ocean under sea ice*. J Geophys Res. **97**(C4) 5365-5379
- Mellor G.L. and T. Yamada (1974). *A hierarchy of turbulence closure models for planetary boundary layers*. J. Atmos. Sciences **31**, 1791-1806
- Mellor G.L. and T. Yamada (1982). *Development of a turbulence closure model for geophysical fluid problems*. Rev. Geophys. Spac. Phys. **20**(4), 851-875
- Mellor G.L., M.G. McPhee and M. Steele (1986). *Ice-seawater turbulent boundary layer interaction with melting or freezing*. J. Phys. Oceanogr. **16**, 1829-1846
- Mellor G.L. and L. Kantha (1989). *An ice-ocean coupled model*. J. Geophys. Res. **94**(C8), 10937-10954

- Mesinger F. and A. Arakawa (1976). *Numerical methods used in atmospheric models*. WMO-ISCU Joint Organizing Committee, GARP Publications Series **17**
- Mestas-Nuñez A.M., D.B. Chelton, M.H. Freilich and J.C. Richman (1994). *An evaluation of ECMWF-based climatological wind stress fields*. *J. Phys. Oceanogr.* **24**, 1532-1549
- Morales Maqueda M.A. (1995). *Un modelo acoplado del hielo de mar y del oceano superficial para estudios climaticos*. PhD Thesis, Univesidad Complutense Madrid, Spain, 426 pp.
- Morawitz W.M.L., P.J. Sutton, P.F. Worcester and B.D. Cornuelle (1996). *Three-dimensional observations of a deep convective chimney in the Greenland Sea during winter 1988/1989*. *J. Phys. Oceanogr.* **26**, 2316-2343
- Muench R.D. and A.L. Gordon (1995). *Circulation and transport of water along the western Weddell Sea margin*. *J. Geophys. Res.* **100**(C9), 18503-18515
- Murray F.W. (1967). *On the computation of saturation vapor pressure*. *J. Appl. Meteorol.* **6**, 203-204.
- Oberhuber J.M. (1988). *An atlas based on the COADS data set: the budgets of heat, buoyancy and turbulent kinetic energy at the surface of the global ocean*. Max-Planck-Institut für Meteorologie, Rep 15, Hambourg, Germany, 194pp.
- Oey L.-Y. and G.L. Mellor (1993). *Subtidal variability of estuarine outflow, plume, and coastal current: a model study*. *J. Phys. Oceanogr.* **23**, 164-171
- Overland J.E. and P.S. Guest (1991). *The Arctic snow and air temperature budget over sea ice during winter*. *J. Geophys. Res.* **96**(C3) 4651-4662
- Pacanowski R.C. and S.G.H. Philander (1981). *Parameterization of vertical mixing in numerical models of tropical oceans*. *J. Phys. Oceanogr.* **11**, 1443-1451
- Parkinson C.L. and W.M. Washington (1979). *A large-scale numerical model of sea ice*. *J. Geophys. Res.* **84**(C1), 311-336
- Parmerter R.R. and M.D. Coon (1972). *Model of pressure ridge formation in sea ice*. *J. Geophys. Res.* **77**(33), 6565-6575
- Payne R.E. (1972). *Albedo of the sea surface*. *J. Atmos. Sci.* **29**, 959-970
- Philander S.G.H. and R.C. Pacanowski (1986). *A model of the seasonal cycle in the tropical Atlantic Ocean*. *J. Geophys. Res.* **91**(C12), 14192-14206
- Prather M.C. (1986). *Numerical advection by conservation of second-order moments*. *J. Geophys. Res.* **91**(D6), 6671-6681
- Reason C.J.C. and S.B. Power (1994). *The influence of the Bering Strait on the circulation in a coarse resolution global ocean model*. *Clim. Dyn.* **9**, 363-369
- Reed R.K. (1977). *On estimating insolation over the ocean*. *J. Phys. Oceanogr.* **7**, 482-485
- Roberts M.J., R. Marsh, A.L. New and R.A. Wood (1996). *An intercomparison of a Bryan-Cox-type ocean model and an isopycnic ocean model. Part I : The subpolar gyre and high-latitude processes*. *J. Phys. Oceanogr.* **26**, 1495-1527
- Rodi W. (1987). *Examples of calculation methods for flow and mixing in stratified fluids*. *J. Geophys. Res.* **92**(C5), 5305-5328

- Rood R.B. (1987). *Numerical advection algorithms and their role in atmospheric transport and chemistry models*. Rev. Geophys. **25**, 71-100,
- Rosati A. and K. Miyakoda (1988). *A general circulation model for upper ocean simulation*. J. Phys. Oceanogr. **18**, 1601-1626
- Semtner A.J. (1976). *A model for the thermodynamic growth of sea ice in numerical investigations of climate*. J. Phys. Oceanogr. **6**, 379-389
- Send U. and J. Marshall (1995). *Integral effects of deep convection*. J. Phys. Oceanogr. **25**, 855-872
- Simmons I. and M. Dix (1989). *The use of mean atmospheric parameters in the calculation of modeled mean surface heat fluxes over the world's oceans*. J. Phys. Oceanogr. **19**, 205-215
- Simonot J.-Y. and H. LeTreut (1986). *A climatological field of mean optical properties of the world ocean*. J. Geophys. Res. **91**(C5), 6642-6646
- Simonsen K. and P.M. Haugan (1996). *Heat budgets of the Arctic Mediterranean and sea surface heat flux parameterizations for the Nordic Seas*. J. Geophys. Res. **101**(C3), 6553-6376
- Simpson J.J. and C.A. Paulson (1979). *Mid-ocean observations of atmospheric radiation*. Quart. J. R. Met. Soc. **105**, 487-502.
- Shine K.P. (1984). *Parameterization of the shortwave flux over high albedo surfaces as a function of cloud thickness and surface albedo*. Quart. J. R. Met. Soc. **110** 747-764
- Shine K.P. and A. Henderson-Sellers (1985). *The sensitivity of a thermodynamic sea ice model to changes in surface albedo parameterization*. J. Geophys. Res. **90**(D1), 2243-2250
- Shirasawa K. and R.G. Ingram (1991). *Characteristics of the turbulent oceanic boundary layer under sea ice. Part I : a review of the ice-ocean boundary layer*. J. Mar.Syst. **2**, 153-160
- Smith S.D., R.D. Muench and C.H. Pease (1990). *Polynyas and leads: an overview of physical processes and environment*. J. Geophys. Res. **95**(C6), 9461-9479
- Staneva J.V., E.V. Stanev and N.H. Rachev (1996). *Heat balance estimates using atmospheric analysis data: a case study for the Black Sea*. J. Geophys. Res. **100**(C9), 18581-18596
- Taljaard J.J., H. van Loon, H.L. Crutcher and R.L. Jenne RL (1969) *Climate of the upper air, Part I. Southern Hemisphere, Vol. 1, temperatures, dew points, and heights at selected pressure levels*. U.S. Naval Weather Service, NAVAIR 50-1C-55, Washington D.C., 135pp.
- Thorndike A.S., D.A. Rothrock, G.A. Maykut and R. Colony (1975). *The thickness distribution of sea ice*. J. Geophys. Res. **80**(33), 4501-4513
- Thorndike A.S. (1986a). *Kinematics of sea ice*. In, *The geophysics of sea ice*, N. Untersteiner (editor). NATO ASI Series Vol 146, Plenum Press, New York, USA, 489-549
- Thorndike A.S. (1986b). *Diffusion of sea ice*. J. Geophys. Res. **91**(C6), 7691-7696
- Toulany B. and C. Garrett (1984). *Geostrophic control of fluctuating barotropic flow through straits*. J. Phys. Oceanogr. **14**, 649-655

- Trenberth K.E., J.G. Olson, and W.G. Large (1989). *A global ocean wind stress climatology based on ECMWF analyses*. National Center for Atmos. Res., NCAR/TN-338 +STR, Boulder, Colorado, 93pp.
- Trenberth, K.E. (1992). *Climate System Modeling*. Cambridge University Press, Cambridge, United Kingdom, 788 pp.
- Xie P. and P. A. Arkin (1996). *Analyses of global monthly precipitation using gauge observations, satellite estimates and numerical model predictions*. J. Clim. **9**, 840-858
- Wanninkhof R. (1992). *Relationship between wind speed and gas exchange over the ocean*. J. Geophys. Res. **97**(C5), 7373-7382
- Warner M.J. and R.F. Weiss (1985). *Solubilities of chlorofluorocarbons 11 and 12 in water and seawater*. Deep Sea Res. **32**(12), 1485-1497
- Warner M.J. and R.F. Weiss (1992). *Chlorofluoromethanes in South Atlantic Antarctic Intermediate Water*. Deep Sea Res. **39**(11/12), 2053-2075
- Weare B.C. (1989). *Uncertainties in estimates of surface heat fluxes derived from marine reports over the tropical and subtropical oceans*. Tellus **41A**, 357-370
- Weeks W.F. and S.F. Ackley (1986) *The growth, structure, and properties of sea ice* In, *The geophysics of sea ice*, N. Untersteiner (editor) NATO ASI Series vol 146. Plenum Press, New-York, 9-164
- Zillmann J.W. (1972). *A study of some aspects of the radiation and the heat budgets of the southern hemisphere oceans*. Meteorol. Stud. **26** Bur. Meteorol. Dep. of the Interior, Canberra, Australia, 562 pp.